NASA TECHNICAL NOTE

NASA TN D-2131

NASA TN D-2131

CHEMICAL RELAXATION BEHIND STRONG NORMAL SHOCK WAVES IN CARBON DIOXIDE INCLUDING INTERDEPENDENT DISSOCIATION AND IONIZATION PROCESSES

by John T. Howe and Yvonne S. Sheaffer

Ames Research Center
Moffett Field, California

NATIONAL AERONAUTICS AND SPACE ADMINISTRATION • WASHINGTON, D. C. • FEBRUARY 1964

CHEMICAL RELAXATION BEHIND STRONG NORMAL SHOCK WAVES IN CARBON DIOXIDE INCLUDING INTERDEPENDENT DISSOCIATION AND IONIZATION PROCESSES

By John T. Howe and Yvonne S. Sheaffer

Ames Research Center
Moffett Field, Calif.

NATIONAL AERONAUTICS AND SPACE ADMINISTRATION

For sale by the Office of Technical Services, Department of Commerce,
Washington, D.C. 20230 -- Price $1.50

CHEMICAL RELAXATION BEHIND NORMAL SHOCK W... IN CARBON DIOXIDE INCLUDING INTERDEPENDENT DISSOCIATION AND IONIZATION PROCESSES

By John T. Howe and Yvonne S. Sheaffer

SUMMARY

Collision theory is used to estimate chemical reaction rate coefficients for the dissociation of CO_2 and CO and for the ionization of CO, O, and C. The estimated coefficients are used to obtain solutions for the interdependent dissociation and ionization processes of CO_2 and its components (including eight chemical species) coupled with the fluid flow behind a normal shock wave. Solutions of both the nonequilibrium chemical relaxation region behind the shock wave and the asymptotic equilibrium conditions are obtained for shock speeds ranging from 9 to 20 kilometers per second and ambient densities of 10^{-2} to 10^{-4} standard earth atmosphere density. Results are presented in the form of flow-field profiles of pressure, temperature, density, enthalpy, velocity, species concentration, and relaxation distance behind the shock. In addition, tables and graphs of asymptotic equilibrium properties and composition are presented. The effects of the state of internal excitation on the chemically relaxing flow field are investigated.

INTRODUCTION

The dissociative relaxation of carbon dioxide and its effect on the flow field behind normal shock waves at speeds up to about 10 kilometers per second was examined in references 1 and 2. However, at speeds above (as well as speeds slightly lower than) 10 kilometers per second, ionizing reactions become important to the chemical relaxation process. The charged particles produced by these reactions are of special interest from the point of view of their effects on energy transport in the reacting mixture and on communications blackout problems associated with planetary atmosphere entry.

The present analysis includes dissociation reactions for CO_2 and CO and ionization reactions for CO, C, and O. Thus, results include typical profiles of charged particle concentration in the relaxation region behind the shock where the flow is not in chemical equilibrium as well as the equilibrium concentration of charged particles over a broad range of shock speed and ambient density.

In order to study nonequilibrium chemical effects in CO_2, it is necessary to know something about the reactions which occur and the rates at which they proceed. Although some experimental data on the chemical kinetics of CO_2 exist for temperatures below 2700° K (refs. 3, 4, and 5), we do not know of any definitive experimentally obtained reaction rate data for CO_2 and its components at the high temperatures encountered behind strong shock waves. For this reason, it is

necessary to postulate the chemical reactions and to estimate their rate coefficients with the aid of collision theory, as was the case in references 1 and 2. The reaction rate coefficients are all estimated in the same way and are at least self consistent. The chemical relaxation results obtained with these rate coefficients are considered to be first estimates.

The situation with regard to the prediction of equilibrium properties and composition behind shock waves in CO_2 is considerably better. The equilibrium results presented in the paper do not depend on the reaction rate estimates. The equilibrium properties are obtained by a direct calculation procedure for a specified shock speed and ambient density.

SYMBOLS

A	Avogadro's number
a	defined by equation (A5)
a_{z_i}	number of atoms of type z in species i
B_{c_r}	coefficient in equilibrium coefficient expression (25) for reaction r
B_{f_r}	coefficient in forward reaction rate expression (24) for reaction r
b	defined by equation (A6)
c_p	specific heat at constant pressure (per mass basis)
$\hat{c}_p$	specific heat at constant pressure (per mole basis)
c	defined by equation (A7)
d	average diameter of two colliding particles
E_{c_r}	energy in equilibrium coefficient expression (25) for reaction r
E_{f_r}	activiation energy in forward reaction rate coefficient (24) for reaction r
h	static enthalpy (per mass basis)
$\hat{h}$	static enthalpy (per mole basis)
$\hat{h}_i^o$	enthalpy of formation of species i (per mole basis)
$\underline{\hat{h}_i^o}_l$	defined by equation (A2)
K_{c_r}	equilibrium coefficient for reaction r
k_{f_r}	forward reaction rate coefficient for reaction r

k	total number of species (eq. (4))
M	typical collision partner
$\mathbf{M}_i$	molecular weight of species i
$\mathbf{M}^*$	reduced molecular weight $\left(\frac{1}{\mathbf{M}_i} + \frac{1}{\mathbf{M}_M}\right)^{-1}$
n	$\sum_{i=1}^{k} n_i$, number of moles of mixture per unit mass of mixture
n_i	number of moles of species i per unit mass of mixture
P	transition probability or steric factor
p	static pressure
$\hat{R}$	universal gas constant, 1.98717×10^{-3} kcal/g mole ^{o}K
s	number of classical squared terms of energy contributing to reaction
T	absolute temperature
u	velocity in x direction
X	a chemical species
x	distance behind the shock
α	forward stoichiometric coefficient and exponent in equations (24) and (25)
β	backward stoichiometric coefficient
ϵ	ρ_∞/ρ_s, density ratio across shock
η	defined by equation (34)
ρ	mass density of gas mixture
ρ_o	standard or sea-level atmosphere density, 1.225×10^{-3} g/cm^3
σ	constant in equation (23)

Superscripts

$\wedge$	per mole basis
$-$	equilibrium value

Subscripts

b	backward
f	forward
i	species i; i = 1 through 8 corresponds to CO_2, CO, O, C, CO^+, O^+, C^+, e^-, respectively
l=1	temperatures less than or equal to T_{ref}
l=2	temperatures greater than T_{ref}
M	typical collision partner
o	reference or sea-level condition
r	rth reaction; r = 1 through 5 shown in equations (17) through (21)
ref	reference temperature, 12,500° K
s	conditions immediately behind shock
∞	conditions ahead of shock

ANALYSIS

Differential Equations

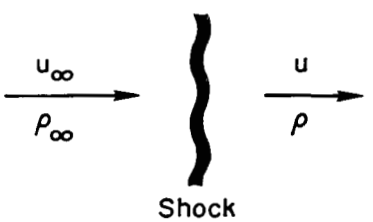

Sketch (a)

The flow model chosen for analysis is that of a normal shock wave moving at velocity, u_∞, into quiescent CO_2 at ambient density, ρ_∞. The corresponding flow field as seen by an observer traveling with the shock is shown in sketch (a).

The equations describing the flow field behind the shock are statements of conservation of mass, the momentum theorem, and conservation of energy and are, respectively,

$$\rho u = \rho_\infty u_\infty = \text{constant} \tag{1}$$

$$\rho u \frac{du}{dx} = - \frac{dp}{dx} \tag{2}$$

and

$$u \frac{du}{dx} + \frac{dh}{dx} = 0 \tag{3}$$

where transport phenomena have been neglected in equations (2) and (3). The enthalpy of the mixture of reacting species is

$$h(p,\rho,n_i \ldots, n_k) = \sum_{i=1}^{k} n_i \hat{h}_i \tag{4}$$

and

$$\hat{h}_i = \int_o^T \hat{c}_{p_i} \, dT + \hat{h}_i^o \tag{5}$$

In equation (4), enthalpy is assumed to be a function of pressure, density, and chemical composition, but not a function of the vibrational or electronic states of the molecules. As in references 1 and 2, behind the shock we assume that the specific heat at constant pressure for each species is constant at its fully excited classical value[1] ($5\hat{R}/2$ for atoms, ions, and electrons, $9\hat{R}/2$ for diatomic molecules, and $7.5\hat{R}$ for linear triatomic molecules (ref. 6)). The equation of state is needed and is

$$p = \rho \hat{R} T \sum_{i=1}^{k} n_i \tag{6}$$

Equations (1), (2), (3), (4), and (6) can be manipulated to yield (refs. 1 and 7)

$$\frac{du}{dx} = \frac{u}{1 - \frac{\rho u^2}{p} \frac{\sum_{i=1}^{k} n_i \left[\left(\frac{\hat{c}_{p_i}}{\hat{R}} \right) - 1 \right]}{\sum_{i=1}^{k} n_i \frac{\hat{c}_{p_i}}{\hat{R}}}} \left(\frac{\sum_{i=1}^{k} \frac{dn_i}{dx}}{\sum_{i=1}^{k} n_i} - \frac{\sum_{i=1}^{k} \frac{\hat{c}_{p_i}}{\hat{R}} \frac{dn_i}{dx}}{\sum_{i=1}^{k} n_i \frac{\hat{c}_{p_i}}{\hat{R}}} - \frac{\sum_{i=1}^{k} \hat{h}_i^o \frac{dn_i}{dx}}{\hat{R}T \sum_{i=1}^{k} n_i \frac{\hat{c}_{p_i}}{\hat{R}}} \right) \tag{7}$$

[1]It is shown in the appendix that, for the high shock speeds considered, this assumption of full vibrational excitation leads to essentially the same results in the equilibrium and most of the nonequilibrium flow field as the assumptions of no vibrational excitation or of complete vibrational and electronic excitation.

which shows coupling between the chemical relaxation processes and the flow field. The chemical rate equations for the reaction r

$$\sum_{i=1}^{k} \alpha_{r,i} X_i \underset{k_{b_r}}{\overset{k_{f_r}}{\rightleftharpoons}} \sum_{i=1}^{k} \beta_{r,i} X_i \tag{8}$$

are expressed in the usual form (ref. 7 or 8)

$$\frac{dn_i}{dx} = \frac{1}{\rho u} \sum_{r} (\beta_{r,i} - \alpha_{r,i}) k_{f_r} \left[\Pi_i (\rho n_i)^{\alpha_{r,i}} - \frac{1}{K_{c_r}} \Pi_i (\rho n_i)^{\beta_{r,i}} \right] \tag{9}$$

If there are m types of atoms in addition to free electrons, $(m + 1)$ of equation (9) can be replaced by m statements of conservation of atoms (in this case carbon and oxygen) of the form

$$\sum_{i}^{k} a_{z_i} n_i = \sum_{i}^{k} a_{z_i} n_{i_s} \tag{10}$$

plus one statement that the number of ions equals the number of electrons (only singly ionized species are considered). In applying equation (10), we consider an atomic ion to be equivalent to 1 atom of the appropriate species. It is noted that equation (10) can be differentiated to provide m values of dn_i/dx for use in equation (7).

Boundary conditions for the flow equations (7), (2), and (3) are obtained from the normal shock relations and are for $x = 0$

$$u = u_s = \epsilon u_\infty \tag{11}$$

$$p = p_s = \rho_\infty u_\infty^2 (1 - \epsilon) \tag{12}$$

$$h = h_s = n_{1_s} (\hat{c}_{p_1} T_s + \hat{h}_1^o) = h_\infty + \frac{1}{2} u_\infty^2 (1 - \epsilon^2) \tag{13}$$

where the strong shock approximations have been used for boundary condition (12), and it has been assumed that CO_2 does not dissociate in passing through the shock wave in boundary condition (13). Consistent with the latter are the boundary conditions on the chemical rate equations (9) which are at $x = 0$

$$n_1 = n_{1_s} = (\mathbf{M}_1)^{-1} \tag{14}$$

$$n_2 = n_3 = n_4 = n_5 = n_6 = n_7 = n_8 = 0 \tag{15}$$

Combining boundary conditions (11), (12), (13), and the equation of state (6) yields the expression for ϵ needed for evaluating the boundary conditions (11), (12), and (13)

$$\epsilon = \left(2 \frac{\hat{c}_{p_1}}{\hat{R}} - 1 \right)^{-1} \tag{16}$$

The set of differential equations with their boundary conditions describing the interrelated chemical and flow processes in that part of the flow field behind the shock that is not in chemical equilibrium is thus complete, and we turn our attention to the chemical reactions themselves and the rates at which they proceed.

Chemical Reactions

The reactions assumed for the dissociation, ionization, and recombination of CO_2 and its components are

$$r = \begin{cases} 1 & CO_2 + M \rightleftarrows CO + O + M & (17) \\ 2 & CO + M \rightleftarrows C + O + M & (18) \\ 3 & CO + M \rightleftarrows CO^+ + e^- + M & (19) \\ 4 & O + M \rightleftarrows O^+ + e^- + M & (20) \\ 5 & C + M \rightleftarrows C^+ + e^- + M & (21) \end{cases}$$

where M is a typical collision partner. Although it may be expected that electrons are more efficient than the large particles in producing ionizing reactions, no attempt is made to distinguish between electrons and larger particles as collision partners[2] and

$$n_M = n \tag{22}$$

[2]For argon, it is generally agreed that electron collision partners are important to the rate at which equilibrium is approached behind shock waves, although there is little agreement as to the mechanism for initiating ionization (refs. 9 - 13).

For air at shock speeds up to 10 km/sec, ionizing processes listed in order of decreasing importance are atom-atom collisions, photoionization, electron impact, atom-molecule, and molecule-molecule collisions according to reference 14. However, the importance of electron impact is increasing with shock speed.

For carbon dioxide, although the ionization rate coefficients with electron collision partners are conceivably an order of magnitude larger than those with large particle collision partners, we do not know either within an order of magnitude and thus do not attempt to distinguish between them.

The rate at which reactions (17) through (21) proceed to the right is characterized by the forward reaction rate coefficient expressed either in the form given by collision theory

$$k_{f_r} = \frac{2PAd^2}{\sigma(s-1)!}\left(\frac{2\pi\hat{R}T}{M^*}\right)^{1/2}\left(\frac{E_{f_r}}{\hat{R}T}\right)^{s-1} e^{-(E_{f_r}/\hat{R}T)} \tag{23}$$

or in the Arrhenius form

$$k_{f_r} = B_{f_r} T^{\alpha_{f_r}} e^{-(E_{f_r}/\hat{R}T)} \tag{24}$$

The backward reaction rate is included in the equilibrium coefficient

$$K_{c_r} = \frac{k_{f_r}}{k_{b_r}} = \bar{\rho}\prod_{i=1}^{k} \bar{n}_i^{\beta_{r,i}-\alpha_{r,i}} = B_{c_r} T^{\alpha_{c_r}} e^{-(E_{c_r}/\hat{R}T)} \tag{25}$$

Subsequently, we want to calculate the chemical equilibrium conditions which the chemically relaxing flow approaches asymptotically.

Equilibrium Conditions

The 13 equilibrium properties of interest include the flow velocity $\bar{u}$, thermodynamic properties $\bar{p}$, $\bar{\rho}$, and $\bar{T}$, and chemical concentrations $\bar{n}$, $\bar{n}_1 \ldots \bar{n}_8$. They are obtained from the simultaneous solution of the following 13 algebraic equations. By definition

$$\bar{n} = \sum_{i=1}^{8} \bar{n}_i \tag{26}$$

Statements of conservation of oxygen and carbon atoms are

$$\bar{n}_3 = 2n_{1_S} - 2\bar{n}_1 - \bar{n}_2 - \bar{n}_5 - \bar{n}_6 \tag{27}$$

and

$$\bar{n}_4 = n_{1_S} - \bar{n}_1 - \bar{n}_2 - \bar{n}_5 - \bar{n}_7 \tag{28}$$

The number of moles of electrons equals the number of moles of ions and therefore

$$\bar{n}_8 = \bar{n}_5 + \bar{n}_6 + \bar{n}_7 \tag{29}$$

The equation of state is

$$\frac{\bar{p}}{\bar{\rho}} = \bar{n}\hat{R}\bar{T} \tag{30}$$

The strong shock relations give

$$\bar{p} = \rho_\infty u_\infty (u_\infty - \bar{u}) \tag{31}$$

$$n_{1_s}\hat{h}_1^o + \frac{1}{2}(u_\infty^2 - \bar{u}^2) = \sum_{i=1}^{8} \bar{n}_i \left[\left(\frac{\hat{c}_{p_i}}{\hat{R}}\right)\hat{R}\bar{T} + \hat{h}_i^o\right] \tag{32}$$

$$\bar{u} = \frac{\rho_\infty u_\infty}{\bar{\rho}} \tag{33}$$

The remaining five equations will not be listed, but are simply equation (25) written for the five reactions (17) through (21).

Method of Solution

Solutions for the nonequilibrium flow field were obtained by numerical integration of the differential equations (2), (3), (7), and (9) subject to boundary conditions (11) through (15) making use of equations (1), (6), and (16). The integration was performed on the IBM 7090 digital computer, making use of the Adams-Moulton predictor-corrector variable step integration scheme (ref. 15). Values of dissociation energy and some of the other physical constants employed in the analysis were either obtained or estimated from information in references 16 and 17. The rate and equilibrium coefficients will be presented subsequently.

The set of 13 equilibrium equations ((26) through (33) plus the five eqs. (25) in which r takes on the value 1 through 5), some of which are nonlinear and transcendental, were solved in a direct way by the Newton-Raphson method (ref. 18, p. 213). In addition, the results were verified by the method of tracing the locus of roots described in reference 19.

DISCUSSION OF RESULTS

The results of the chemical reaction rate coefficient estimates, and equilibrium coefficient and equilibrium property computation are presented first. Subsequently, some typical nonequilibrium chemical and flow field profiles and the relaxation distance are presented and discussed.

Chemical Kinetics and Equilibrium Results

Reaction rate coefficients.- The estimated values of the constants in the forward reaction rate coefficients were obtained with the aid of collision theory and are listed in table I in the Arrhenius form (eq. (24)). As in references 1 and 2, it has been assumed for present purposes that $P = s = 1$ in the forward reaction rate coefficient expression (23), and that the activation energy equals the reaction energy. An equivalent assumption is that collision of pairs having total energy in a specific degree of freedom (such as translation) equal to or greater than the reaction energy will result in a reaction (ref. 20). The neglected effect that reaction rates tend to be lowered because not every such collision results in a reaction (i.e., P is actually less than unity) is compensated to some extent by the neglected effect that reaction rates tend to be raised because more than one degree of freedom may participate in the reaction (i.e., s is actually greater than 1). For these reasons (which are discussed more fully in ref. 1) and for lack of experimental evidence, we estimate reaction rates in accord with the above assumption, and the result appears in figure 1.

At a temperature of about 20,000° K, the rate coefficients of the various reactions exhibit rather large over-all differences ($\sim 10^2$ for example). Since the colliding pairs (electrons excepted) do not differ greatly in size or molecular weight, the large spread in the rate coefficients at low temperatures is attributable to differences in the activation energy E_{f_r} which appears as part of the exponent in equation (24). At high temperatures, however, the entire exponent $E_{f_r}/\hat{R}T$ is small so that differences in activation energy are of diminishing importance and $k_{f_r} \sim T^{\alpha_{fr}}$ ($\sim T^{1/2}$ in accord with the assumption $s = 1$). Thus at a high temperature, the various reaction rate coefficient estimates do not differ greatly from one another (they differ by a factor of less than 2 at 150,000° K) as can be seen in the figure. The coefficients over this entire temperature range were required for estimation of the flow profiles in the nonequilibrium zone discussed below.

Equilibrium results.- The equilibrium coefficients were obtained by empirically fitting data obtained from references 16 and 17 by use of the far right side of equation (25). The resulting values of the parameters in equation (25) are shown in table I, and the equilibrium coefficients themselves are shown in figure 2.

A summary of the equilibrium composition and properties behind normal shock waves obtained by use of the equilibrium coefficients and equations (26) through (33) (plus five eqs. (25)) is presented in table II. Two values of each equilibrium property are presented for each shock speed and ambient density. The two values are identified by "index" 1 and 2 corresponding, respectively, to the fully excited classical specific heat assumption and a "revised model" for specific heat presented in the appendix. The two values do not differ from one another to a significant extent.

A few of the equilibrium properties behind the shock wave are presented graphically in figures 3 through 6. Equilibrium values of pressure and enthalpy are not presented because they are almost the same as the nonequilibrium values

occurring just behind the shock calculated by equations (12) and (13), respectively. On the other hand, values of equilibrium density and temperature are quite different from the nonequilibrium properties just behind the shock wave. Equilibrium density is shown as a function of ambient density and shock speed in figure 3. It is seen to be a relatively weak function of shock speed. It can be seen that $\bar{\rho}/\rho_\infty$ would be about the same for all of these cases. It varies from about 21 (at 9 km/sec for $\rho_\infty = 1.225\times10^{-7}$ g/cm^3) to about 11 (at 20 km/sec for $\rho_\infty = 1.225\times10^{-5}$ g/cm^3). At the lowest ambient density in figure 3 ($\rho_\infty = 1.225\times10^{-7}$ g/cm^3) the curve has been cut off at 15 km/sec because doubly ionized species, which have been neglected, should be present in appreciable quantities. The values of equilibrium temperatures are presented in the same way in figure 4.

The concentration of free electrons is of special interest from the point of view of both convective and radiative heating, and communications blackout problems associated with planetary atmosphere entry. Equilibrium electron concentrations in terms of mole fractions are presented in figure 5. The limiting concentration is 0.5 for electrons (or ions) because only singly ionizing reactions were considered. The actual equilibrium number concentration of electrons (or ions) is shown in figure 6. For ambient density of 10^{-7} to 10^{-5} g/cm^3, the number of free electrons (or ions) varies from about 5×10^{14} to 5×10^{18} per cubic centimeter over the speed range 9 to 20 km/sec.

Chemically Relaxing Flow Field

Profiles of thermodynamic, kinematic and chemical quantities in the nonequilibrium part of the flow field behind the shock were obtained by integration of equations (2), (3), (7), and (9) subject to their boundary conditions and with the use of the chemical rate coefficient estimates.

A solution for a high shock speed and low ambient density (15 km/sec and $\rho_\infty/\rho_o = 10^{-4}$, respectively) is shown in figure 7. In figure 7(a), all quantities have been made dimensionless with respect to their values immediately behind the shock wave. As chemical relaxation proceeds (increasing x), temperature diminishes monotonically. On the other hand, particle velocity first increases and then decreases while density varies in the opposite way with increasing distance behind the shock wave. This behavior has been discussed in reference 1. The variation of pressure and enthalpy in the flow field is very small as would be expected from the appendix of reference 1.

The mole fraction profiles of the eight chemical species are shown in figure 7(b). It is seen that CO_2 vanishes a short distance behind the shock wave. Both CO and O rapidly increase in concentration for a short distance behind the shock wave and then diminish because of further dissociation and ionization processes. Electrons are the predominant species in the flow field

for x greater than half a millimeter.[3] Although the nonequilibrium electron concentration has overshot the equilibrium value, it does approach that value when x is large. This behavior will be observed in subsequent examples as well. It is interesting to see that the concentration of atomic oxygen remains high in much of the relaxation region.

Profiles for a lower shock speed (9 km/sec) at the same low ambient density ($\rho_\infty/\rho_o = 10^{-4}$) are shown in figure 8. It is noted that the density is far from its equilibrium value 10 cm behind the shock (fig. 8(a)). The dominant species in most of the relaxation region is atomic oxygen (fig. 8(b)). Interestingly, it achieves an almost constant value only 3 mm behind the shock in spite of the fact that CO is still dissociating into C and O. Thus the ionization of atomic oxygen keeps pace with the production of atomic oxygen throughout most of the relaxation region. The concentration of electrons and ions is relatively small at this low shock speed. This figure may be compared with figure 5 of reference 1, in which ionization reactions were neglected. The thermodynamic and flow-field structure is much the same in either case, although the over-all concentration of the nonionized species is higher in that reference, as would be expected.

Results for a high-speed shock wave (u_∞ = 15 km/sec) at an intermediate ambient density level ($\rho_\infty/\rho_o = 10^{-3}$) are shown in figure 9. The result is much like that of figure 7 at the same speed, but a decade lower ambient density. The comments pertaining to figure 7 also apply to figure 9, except that the chemical relaxation takes place in a shorter distance behind the shock.

Finally, examples for high- and low-speed shock waves at ambient density still another decade higher are shown in figures 10 and 11. The same general comments apply as in figures 7 and 8. The relaxation distance is considerably shorter at this higher density. It is interesting to observe for the low-speed example of figure 11 that some electrons are produced in the relaxation region, but that they tend to recombine with ions as the flow approaches equilibrium.

The results of a large number of examples can be summarized in terms of a chemical relaxation distance.

Relaxation Distance

The chemical relaxation distance can be defined as the distance behind the shock wave at which the over-all chemical relaxation has gone a given fraction (or percentage) toward completion. The fraction of reaction completion is defined in terms of the total change in the number of moles per unit mass occurring in the distance x divided by the total change in number of moles per unit

---

[3]It should be noted that the electron concentration in all of the nonequilibrium profiles to be presented is probably slightly lower than it should be because doubly ionizing reactions have been neglected. However, for the ambient conditions considered in this analysis, doubly ionized species would tend to disappear as equilibrium is approached.

mass required to achieve chemical equilibrium and is

$$\eta = \frac{\sum_{i=1}^{k} n_i - n_{1_s}}{\sum_{i=1}^{k} \bar{n}_i - n_{1_s}} = \frac{n - n_{1_s}}{\bar{n} - n_{1_s}} \tag{34}$$

In all of the examples that were studied, n and, thus, η were monotonic throughout the relaxation region in spite of the fact that n_i is not monotonic for several species.

Countours of the relaxation distance for $\eta = 0.5$, 0.8, and 0.9 are plotted in coordinates of shock speed and ambient density in figures 12, 13, and 14, respectively. These were obtained by interpolation of the solutions. It is seen in figure 12 that the distance for 50-percent reaction completion is quite short; not more than 10^{-1} cm for the entire range of shock conditions shown. The distance for 80-percent reaction completion is roughly a decade higher than for 50-percent completion as noted by comparing figures 13 and 12. Finally, the relaxation distance for 90-percent reaction completion is quite large, ranging from 10^{-2} to 10^{2} cm over the entire range of shock conditions.

It is worth mentioning that these relaxation distances are not very sensitive to the reaction rate assumptions. It was noted in reference 1 that a two to three order of magnitude change in reaction rates results in only a one order of magnitude change in relaxation distance.

CONCLUDING REMARKS

The interdependent dissociative and ionizing chemical rate processes behind shock waves in carbon dioxide have been examined for shock speeds from 9 to 20 km/sec at ambient densities of 10^{-2} to 10^{-4} standard earth atmosphere density. Because of a lack of reaction rate data for carbon dioxide and its components, reaction rate coefficients have been estimated with the aid of some simplifying assumptions and collision theory. The effects of chemical relaxation on the flow field behind normal shock waves have been studied by use of the coupled fluid flow and chemical rate equations.

Results have been presented for both the equilibrium and nonequilibrium regimes behind the shock wave. At the higher speeds (15 km/sec), electrons are the predominant species in most of the nonequilibrium chemical relaxation region. Atomic oxygen is the predominant species in the lower speed examples and is also present in high concentration at the higher speeds.

Equilibrium concentration of electrons is presented in terms of mole fraction of the mixture and in terms of number of electrons per unit volume.

The equilibrium concentration varies from about 5×10^{14} to 5×10^{18} electrons/cc for a shock speed of 9 km/sec at a density of 10^{-4} standard earth atmosphere density to 20 km/sec at a density of 10^{-2}.

Results are also presented in the form of a chemical relaxation distance behind the shock wave. The relaxation distance for 90 percent chemical reaction completion varies from 10^{-2} to 10^{2} cm for an ambient density range of 10^{-2} to 10^{-5} standard earth atmosphere density.

The nonequilibrium results obtained are considered to be preliminary estimates for a number of reasons. They are based on estimates of chemical reaction rate coefficients. Indeed, it is not certain that the reactions studied are the correct reactions. Not all of the conceivable reactions have been included in the analysis. The equilibrium results are in a somewhat better situation in that they are independent of any estimates of reaction rate coefficients. They are not influenced significantly by internal excitation phenomena for the high shock speeds considered.

Interestingly enough, the influence of the state of internal excitation on most of the chemically relaxing flow field is small insofar as this influence is manifested through the thermodynamics of the problem. However, it is possible that dissociation and ionization processes may proceed more readily from excited states, in which case the internal state of excitation would be important in the entire chemical relaxation region.

There is a small part of the nonequilibrium flow field just behind the shock wave in which the state of internal excitation of the various species has a strong influence on the flow properties. This region is likely to be quite important to nonequilibrium radiation problems; thus a knowledge of both the chemical and internal relaxation is important at high temperatures.

Knowledge of the behavior of these common chemical substances at elevated temperature is very meager in spite of the fact that they have long been important species in many combustion problems. The behavior of these substances has acquired new significance relating to planetary entry problems. There is much to be learned both from the macroscopic and the subatomic points of view.

Ames Research Center
National Aeronautics and Space Administration
Moffett Field, Calif., Oct. 23, 1963

APPENDIX

DISCUSSION OF SPECIFIC HEAT ASSUMPTION

The total enthalpy of a reacting gas mixture behind a shock wave is essentially fixed by the free-stream velocity. Similarly, pressure is determined by the free-stream density and velocity. The local temperature (and, indirectly, the density, particle velocity, and composition) of the reacting gas mixture behind the shock wave for a given total enthalpy (and set of reaction rate coefficients) is dependent on the specific heat assumption. In this paper, the specific heat of each species was assumed constant at its fully excited classical value. However, the effective specific heat of polyatomic species at elevated temperatures behind strong shock waves may be less than the fully excited classical value if the residence time is not sufficient for vibrational degrees of freedom to become excited. Conversely, the specific heat may be higher than the classical value if electronic states become excited. The two extremes, no vibrational excitation, and complete vibrational and electronic excitation, are examined in the following.

VIBRATIONAL EFFECTS

Although vibrational relaxation is rapid compared with dissociative relaxation in CO_2 at lower temperatures (at least for temperatures below 3000° K according to ref. 4), the two rates may be comparable at higher temperatures. For shocked mixtures of O_2 in a bath of Ar, the vibrational and dissociative relaxation rates are comparable at temperatures above 8000° K and the dissociation rate appears to be diminished by at least a factor of 2 where vibration is not in equilibrium (ref. 21).

To some extent, we can assess the importance of vibrational excitation by examining the flow-field modifications corresponding to no vibrational excitation. This is accomplished by simply using the appropriate constant specific heat value for each species in the computation. The result is shown in figures 15 and 16, which can be compared with the full vibrational excitation results shown in the corresponding figures 7 and 10. It will be noted that although the flow-field profiles u/u_s, ρ/ρ_s, and $\overline{T}/T_s$ are considerably different in corresponding figures, the concentration profiles are almost the same. The flow-field profiles differ partly because their reference values u_s, ρ_s, and T_s differ. It will be shown subsequently that except for very close behind the shock, the actual profiles of u, ρ, and T are almost the same for no vibrational and complete vibrational excitation and that the profiles for the mole fraction and for the total number of moles are also much alike for these two conditions.

ELECTRONIC EXCITATION EFFECTS

Electronic excitation effects may be shown by use of a modified model for species enthalpy as follows. The solid lines in figures 17(a) through (f) are the enthalpies of the species CO, O, C, CO^+, O^+, and C^+ obtained from reference 17, based on information from references 16, 22, 23, and 24. The enthalpies of the species CO_2 and e^- are not included because the former is only known with reasonable certainty at relatively low temperatures (~5,000° K according to ref. 17) and the latter is simply obtained by use of its classical specific heat ($\hat{c}_{p_s}/\hat{R} = 2.5$). The slopes of the solid lines in the figures are the specific heat at constant pressure for each species. In figure 17(a), the slope of the CO enthalpy curve for temperatures below about 11,000° K corresponds to the classical value for a diatomic molecule that is fully excited in translation, rotation, and vibration. At higher temperatures, however, the specific heat (or slope) is higher than the fully excited classical value because electronic states have also been excited. The other species shown in figure 17 exhibit similar behavior (to a lesser extent than CO).

To some extent we can evaluate the effects of electronic excitation by comparing the results obtained in the paper by use of the species enthalpy model shown in sketch (b) with those obtained by use of revised model shown in

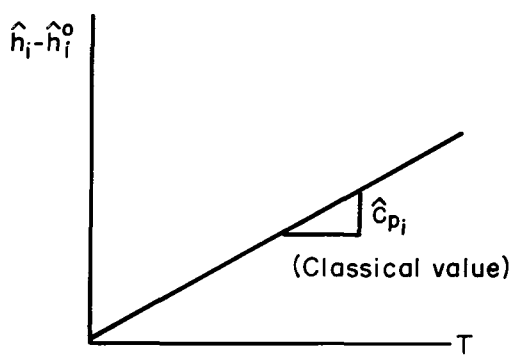

Sketch (b)

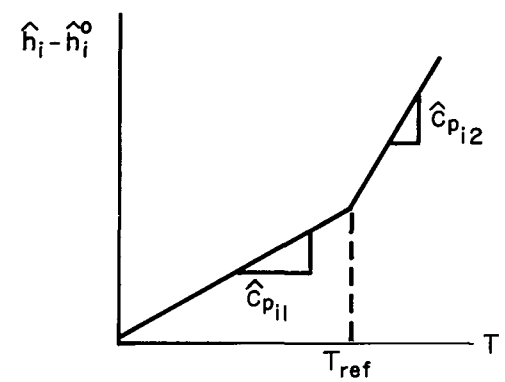

Sketch (c)

sketch (c). The revised model is shown in figure 17 and approximates part of the solid lines by the dashed lines shown. Thus the enthalpy curve is replaced by two straight line segments characterized by two values of specific heat $c_{p_{i_1}}$ and $c_{p_{i_2}}$.

The revised model is very readily included in the analysis in the following way. Equation (5) is revised to read

$$\hat{h}_i = c_{p_{i_l}} T + \underline{\hat{h}_{i_l}^o} \tag{A1}$$

where

$$\underline{\hat{h}_{i_l}^o} \equiv \hat{h}_i^o + (\hat{c}_{p_{i_1}} - \hat{c}_{p_{i_l}})\, T_{ref} \tag{A2}$$

[1]

[1]For convenience, T_{ref} was selected to be 12,500° K for all species.

For $T \leq T_{ref}$, $l = 1$ (and $\underline{\hat{h}^{\circ}_{i_l}} = \hat{h}^{\circ}_i$ as before), while for $T > T_{ref}$ $l = 2$ and expression (A2) is used to evaluate $\underline{\hat{h}^{\circ}_{i_l}}$. The procedure for solving the flow equations is changed only to the extent that two sets of values $\underline{\hat{h}^{\circ}_{i_l}}$ are used to replace $\hat{h}^{\circ}_i$ and two sets of values $\hat{c}_{p_{i_l}}$ are used to replace $\hat{c}_{p_i}$ corresponding to $T \leq T_{ref}$ or $T > T_{ref}$. The chemical rate equations are unchanged.

The calculation of the boundary conditions is changed slightly.[2] For examples of current interest, $T_s > T_{ref}$ so that $\hat{h}^{\circ}_i$ in equation (13) is replaced by $\underline{\hat{h}^{\circ}_{i_2}}$ while ϵ is the positive root of the equation

$$\epsilon = \frac{-b \pm \sqrt{b^2 - 4ac}}{2a} \tag{A3}$$

which is closest to

$$\epsilon \approx \left(\frac{2\hat{c}_{p_{1_2}}}{\hat{R}} - 1 \right)^{-1} \tag{A4}$$

where

$$a = \frac{2\hat{c}_{p_{1_2}}}{\hat{R}} - 1 \tag{A5}$$

$$b = -\frac{2\hat{c}_{p_{1_2}}}{\hat{R}} \tag{A6}$$

and

$$c = \left[1 - \frac{2n_{1_s} T_{ref} \hat{c}_{p_{1_2}}}{u_\infty^2} \left(1 - \frac{\hat{c}_{p_{1_1}}}{\hat{c}_{p_{1_2}}} \right) \right] \tag{A7}$$

Only a minor change is made in the computation of equilibrium conditions. In equation (32), the $\hat{h}^{\circ}_1$ on the left side is unchanged, while $\hat{c}_{p_i}$ and $\hat{h}^{\circ}_i$ on the right side are replaced by $\hat{c}_{p_{i_l}}$ and $\underline{\hat{h}^{\circ}_{i_l}}$, respectively. In the computation, the proper value for l is determined either by previous experience or by judging whether or not $\overline{T} \leq T_{ref}$ by examining the solutions of the nonequilibrium flow field for suitably large values of x.

---

[2]Actually the boundary conditions are changed in form only. For lack of better information of $\hat{c}_{p_{i_2}}$ (for CO_2) at high temperatures, it was set equal to $\hat{c}_{p_{i_1}} = 7.5\hat{R}$, and numerically the boundary conditions are unchanged from those for full classical vibrational excitation in the text.

Equilibrium results obtained by use of the revised model are shown in table II on the lines marked as index 2. In each case they can be compared with the results of the fully excited classical model marked as index 1. It is seen that insofar as equilibrium properties are concerned, the differences between the two models are negligible in the range of shock speed and ambient density under consideration.

Nonequilibrium results obtained by use of the revised model are shown in figures 18 and 19 for a shock speed of 15 km/sec at ambient densities of 10^{-4} and 10^{-2}, respectively. A comparison of these figures with figures 7 and 10, respectively, shows that the chemical concentration profiles in both the classical full vibrationally excited model and the revised electronically excited model are about the same. These comments apply for shock speeds other than that shown.

Now it is instructive to compare the results for no vibration, full vibration, and full vibration plus electronic excitation in a slightly different manner. This is done in figure 20 for shock speed of 15 km/sec and $\rho_\infty/\rho_o = 10^{-4}$. This time the ordinates in figure 20 are not made dimensionless. The flow-field quantities u, ρ, and T differ among the three cases for a short distance behind the shock (about 0.1 cm or less), but are very close to one another over the major portion of the relaxation region. Indeed, density and particle velocity profiles do not differ by more than about 15 percent, while temperature differs by less than 5 percent for $x > 0.1$ cm. In figure 20(b), n the total number of moles per unit mass and n_e the electron mole per unit mass profiles do not differ by more than 6 and 16 percent among the various cases for $x > 0.1$ cm.

It may be expected that for these high-speed shock conditions the equilibrium species would be single particle species. Therefore, the assumptions regarding specific heat would not be expected to have a significant effect on equilibrium conditions. However, it is somewhat surprising that these assumptions have a negligible effect on most of the relaxation region. One reason for the insensitivity of the relaxation profiles might be as follows. Differential equation (9) can be written[3] to show that

$$\frac{dn_i}{dx} \sim k_{f_r}(T)\rho^2$$

Starting with a given n_i, if T or k_{f_r} is altered in one direction by a specific heat assumption, ρ^2 is likely to be altered in the opposite direction and tends to compensate. It follows that since these dn_i/dx are not changed substantially, neither is du/dx (eq. (7)), ρ (eq. (1)), or T (eq. (6)). Also p is almost invariant.

In summary, the effects of the specific heat assumption are felt for only a small distance behind the shock wave. The pressure, enthalpy, density, particle velocity, temperature, mole fraction, and total number of moles per unit mass profiles are almost the same through most of the chemical relaxation region for high shock speed whether there is no vibrational excitation, full vibrational

[3]The backward reaction is neglected.

excitation, or full vibrational and electronic excitation. In short, the influence of the thermodynamics on the chemical relaxation (and relaxation distance) is small.

In obtaining this result, we have assumed that the reactions and their estimated rate coefficients are those presented in the paper and have implicitly assumed that dissociation and ionization proceed with equal probability from any state of excitation. This may not, in fact, be the case. If it is not, additional reactions for excitation or different rate coefficients would have to be employed. Thus the effect of the state of internal excitation of the various species would manifest itself on the chemically relaxing flow field through the reactions and their rate coefficients rather than through the thermodynamics.

REFERENCES

1. Howe, John T., Viegas, John R., and Sheaffer, Yvonne S.: Study of the Nonequilibrium Flow Field Behind Normal Shock Waves in Carbon Dioxide. NASA TN D-1885, 1963.

2. Howe, John T., and Viegas, John R.: Dissociative Relaxation of CO_2 Behind Normal Shock Waves. Paper presented at Interplanetary Missions Conference of 9th Annual American Astronautical Society Meeting at Los Angeles, Jan. 1963.

3. Brabbs, T. A., Belles, F., and Zlatarich S.: Shock Tube Study of Carbon Dioxide Dissociation Rate. J. Chem. Phys., vol. 38, no. 8, April 1963, pp. 1939-44.

4. Gaydon, A. G., and Hurle, I. R.: Measurement of Times of Vibrational Relaxation and Dissociation Behind Shock Waves in N_2, O_2, Air, CO_2, CO, and H_2. Eighth Symposium (International) on Combustion. Williams and Wilkins, 1962.

5. Davies, Wm. O.: Radiative Energy Transfer on Entry Into Mars and Venus. Armour Research Foundation ARF 1200, Sept. 1962.

6. Wilson, A. H.: Thermodynamics and Statistical Mechanics. Cambridge Univ. Press, 1957, p. 136.

7. Vincenti, W. G.: Calculations of the One-Dimensional Nonequilibrium Flow of Air Through a Hypersonic Nozzle. Stanford Univ. Dept. of Aeronautical Engineering Interim Report to AEDC, May 1961.

8. Penner, S. S.: Chemical Reactions in Flow Systems. Butterworths Scientific Pubs. (London), AGARDograph 7, 1955.

9. Bond, J. W.: Structure of a Shock Front in Argon. Phys. Rev., vol. 105, March 15, 1957, pp. 1683-94.

10. Petschek, H., Byron S.: Approach to Equilibrium Ionization Behind Strong Shocks in Argon. Annals of Physics, vol. 1, no. 3, June 1957, pp. 270-315.

11. Weymann, H. D.: On the Mechanism of Thermal Ionization Behind Strong Shock Waves. Tech. Note BN-144, Institute of Fluid Dynamics and Applied Mathematics, University of Maryland, 1958.

12. Blackman, V. H., and Niblett, G. B. F.: Ionization Processes in Shock Waves. Fundamental Data Obtained From Shock Tube Experiments, A. Ferri, ed. (AGARDograph no. 41), Pergamon Press, 1961, p. 221.

13. Frood, D. G. H.: The Problem of Ionization Relaxation for Moderately Strong Shocks in Monatomic Gases. AGARD Specialist Meeting, High Temperature Aspects of Hypersonic Flow, April 3-6, 1962. T.C.E.A., Rhode St. Genese, Belgium.

14. Lin, S. C., and Teare, J. D.: Rate of Ionization Behind Shock Waves in Air. II. Theoretical Interpretation. Res. Rep. 115, AVCO Everett Research Lab., Sept. 1962.

15. Hildebrand, F. B.: Introduction to Numerical Analysis. McGraw-Hill Book Co., N. Y., 1956.

16. Gilmore, F. R.: Properties of Air to 24,000° K. Rand Corp. RM-1543, 1955. ASTIA Document AD-84052.

17. Raymond, J. L.: Thermodynamic Properties of Carbon Dioxide to 24,000° K with Possible Application to the Atmosphere of Venus. Rand Corp. RM 2292, Nov. 1958.

18. Scarborough, J. B.: Numerical Mathematical Analysis. Fifth ed., Johns Hopkins Press, 1958.

19. Klopfenstein, R. W.: RCA Tech. Rep. PTR 949, Sarnoff Research Ctr., RCA, Princeton, N. J.

20. Lewis, Bernard, and Von Elbe, G.: Combustion Flames and Explosions of Gases. Second ed., Academic Press, 1961, p. 5.

21. Camac, M., and Vaughan, A.: Oxygen Vibration and Dissociation Rates in Oxygen-Argon Mixtures. Res. Rep. 84, AVCO Everett Research Lab., Dec. 1959.

22. Woolley, H. W.: Thermodynamic Functions for Carbon Dioxide in Ideal Gas State. Jour. Research U. S. Bureau of Standards, vol. 52, pp. 289-92, 1954.

23. Belzer, Jack, Savedoff, L. S., and Johnston, H. L.: The Thermodynamic Properties of the Gaseous Carbon Monoxide. Tech. Rep. 6, Ohio State Univ. Research Foundation Proj. RF-316, 1953.

24. Moore, Charlotte E.: Atomic Energy Levels. Vol. 1. NBS Circular 467, 1949.

TABLE I.- REACTION RATE AND EQUILIBRIUM COEFFICIENT DATA

r	Reaction	B_{f_r}, $\frac{cm^3}{g\ mol\ sec\ {}^oK^{\alpha_{f_r}}}$	α_{f_r}	E_{f_r}, $\frac{k\ cal}{g\ mol}$	B_{c_r}, $\frac{g\ mol}{cm^3\ {}^oK^{\alpha_{c_r}}}$	α_{c_r}	E_{c_r}, $\frac{k\ cal}{g\ mol}$
1	$CO_2 \rightleftarrows CO + O$	6.955×10^{12}	0.5	125.75	$.17141 \times 10^{13}$	-2.6294	135.73
2	$CO \rightleftarrows C + O$	7.238×10^{12}	.5	256.17	$.17713 \times 10^{7}$	-1.1106	268.57
3	$CO \rightleftarrows CO^+ + e^-$	7.238×10^{12}	.5	323.18	$.41958 \times 10^{-4}$	.72788	333.44
4	$O \rightleftarrows O^+ + e^-$	7.344×10^{12}	.5	314.05	$.42160 \times 10^{-10}$	1.9483	307.73
5	$C \rightleftarrows C^+ + e^-$	7.895×10^{12}	.5	259.84	$.39181 \times 10^{-6}$	1.0415	264.04

TABLE II.- EQUILIBRIUM PROPERTIES BEHIND SHOCK WAVES

Index	ρ_∞, g/cm^3	u_∞, km/sec	$\bar{\rho}$, g/cm^3	$\bar{u}$, km/sec	$\bar{p}$, dyne/cm^2	$\bar{T}$, $^\circ$K	$\bar{n}$, moles/gm	$\bar{n}_1/\bar{n}$	$\bar{n}_2/\bar{n}$	$\bar{n}_3/\bar{n}$	$\bar{n}_4/\bar{n}$	$\bar{n}_5/\bar{n}$	$\bar{n}_6/\bar{n}$	$\bar{n}_7/\bar{n}$	$\bar{n}_8/\bar{n}$	$\bar{n}_8\bar{e}\bar{A}$, electrons/cm^3
1	1.225-7	15	0.21539-5	0.8531	0.25995+6	0.13658+5	0.10622	0.29766-12	0.79778-6	0.25183	0.031581	0.19304-5	0.17597	0.18232	0.35831	0.49389+17
2		15	.21952-5	.8370	.26024+6	.13560+5	.10510	.38401-12	.95924-6	.26337	.033785	.21357-5	.16901	.18240	.35142	.48848+17
1		12.5	.21939-5	.69796	.18072+6	.11453+5	.086466	.21736-10	.22749-4	.47176	.10484	.92752-5	.053772	.15791	.21169	.24194+17
2		12.5	.22276-5	.68739	.18088+6	.11377+5	.085799	.26132-10	.26135-4	.47923	.10961	.98346-5	.050384	.15517	.20556	.23671+17
1		10	.24556-5	.4989	.11639+6	.81813+4	.069646	.32026-7	.60672-2	.64490	.29425	.47410-4	.14682-2	.025875	.027391	.28222+16
2		10	.25280-5	.4846	.11656+6	.80172+4	.069140	.52716-7	.86535-2	.64742	.29829	.51428-4	.11296-2	.021634	.022815	.24025+16
1		9	.26124-5	.4220	.94572+5	.69159+4	.062927	.13080-5	.088641	.63327	.26712	.74633-4	.16902-3	.52437-2	.54874-2	.54348+15
2		9	.26503-5	.4159	.94639+5	.68763+4	.062428	.14951-5	.096936	.63076	.26207	.75370-4	.15606-3	.48822-2	.51135-2	.50973+15
1	1.225-6	20	.14233-4	.17213+1	.44783+7	.27893+5	.13560	.15333-17	.56869-10	.42349-2	.11202-2	.10440-7	.33088	.16644	.49734	.57829+18
2		20	.15891-4	.15418+1	.45223+7	.25390+5	.13474	.27201-16	.40369-9	.95959-2	.21780-2	.34701-7	.32766	.16645	.49412	.63740+18
1		17.5	.17860-4	.12003+1	.34942+7	.19144+5	.12286	.91700-13	.11783-6	.094465	.015181	.10337-5	.27542	.16976	.44517	.58852+18
2		17.5	.18689-4	.11470+1	.35057+7	.18720+5	.12046	.19600-12	.19988-6	.11351	.018254	.14142-5	.26374	.17037	.43410	.58880+18
1		15	.18892-4	.9726	.25775+7	.15948+5	.10284	.85456-11	.33598-5	.27576	.049853	.66453-5	.16610	.17108	.33719	.39470+18
2		15	.19522-4	.9413	.25833+7	.15743+5	.10105	.12419-10	.44091-5	.29429	.054848	.76862-5	.15542	.17000	.32542	.38676+18
1		12.5	.19459-4	.78690	.17936+7	.13164+5	.084169	.36643-9	.64984-4	.48552	.13395	.25401-4	.054294	.13591	.19024	.18772+18
2		12.5	.19916-4	.76886	.17963+7	.13024+5	.083252	.46873-9	.78166-4	.49613	.14114	.27395-4	.049620	.13168	.18133	.18113+18
1		10	.22540-4	.5435	.11584+7	.90038+4	.068621	.39447-6	.013728	.64692	.29838	.11072-3	.14788-2	.018896	.020485	.19089+17
2		10	.23226-4	.5274	.11604+7	.88248+4	.068060	.60745-6	.018672	.64773	.29908	.11812-3	.11667-2	.015971	.017255	.16434+17
1		9	.23637-4	.4664	.94082+6	.77339+4	.061871	.65614-5	.10692	.62715	.25522	.14650-3	.25616-3	.49498-2	.53524-2	.47160+16
2		9	.24007-4	.4593	.94162+6	.76864+4	.061345	.74155-5	.11599	.62438	.24963	.14736-3	.23714-3	.46071-2	.49916-2	.44288+16
1	1.225-5	20	.13514-3	.18129+1	.44558+8	.29919+5	.13248	.17465-13	.13036-7	.022268	.07609-2	.41791-6	.32074	.16474	.48550	.52367+19
2		20	.14898-3	.16445+1	.44971+8	.27912+5	.13001	.11741-12	.48268-7	.038069	.010566	.92738-6	.31148	.16420	.47567	.55508+19
1		17.5	.15523-3	.13810+1	.34555+8	.22824+5	.11725	.86962-11	.10809-2	.13182	.030895	.56776-5	.22575	.16288	.41864	.45906+19
2		17.5	.16511-3	.12983+1	.34732+8	.22179+5	.11402	.18864-10	.18645-5	.15841	.037261	.77952-5	.24014	.16201	.40216	.45614+19
1		15	.16404-3	1.120	.25504+8	.18940+5	.098680	.28254-9	.15098-4	.30478	.076666	.23341-4	.15569	.15355	.30926	.30162+19
2		15	.17299-3	1.062	.25611+8	.18526+5	.096069	.46793-9	.21830-4	.33249	.086467	.28243-4	.14049	.15000	.29051	.29088+19
1		12.5	.17141-3	.89330	.17773+8	.15296+5	.081488	.73332-8	.20385-3	.50438	.16786	.71506-4	.053006	.11070	.16378	.13783+19
2		12.5	.17956-3	.85279	.17835+8	.14941+5	.079918	.11314-7	.28215-3	.52357	.18130	.81083-4	.044694	.10265	.14743	.12746+19
1		10	.20477-3	.5982	.11517+8	.10048+5	.067292	.44250-5	.028585	.64489	.29477	.25087-3	.15795-2	.014048	.015879	.13182+18
2		10	.21084-3	.5810	.11538+8	.98697+4	.066657	.61409-5	.036101	.64407	.29232	.26173-3	.13050-2	.012187	.013754	.11645+18
1		9	.21201-3	.5200	.93492+7	.87538+4	.060560	.34349-4	.13046	.61919	.23985	.28542-3	.38652-3	.45626-2	.52344-2	.40491+17
2		9	.21561-3	.5113	.93587+7	.86952+4	.060012	.38383-4	.14038	.61614	.23368	.28571-3	.35843-3	.42388-2	.48830-2	.38065+17

NOTE: A group of digits followed by -n (or +n) indicates that the decimal point should be n places to the left (or right) of the position shown.

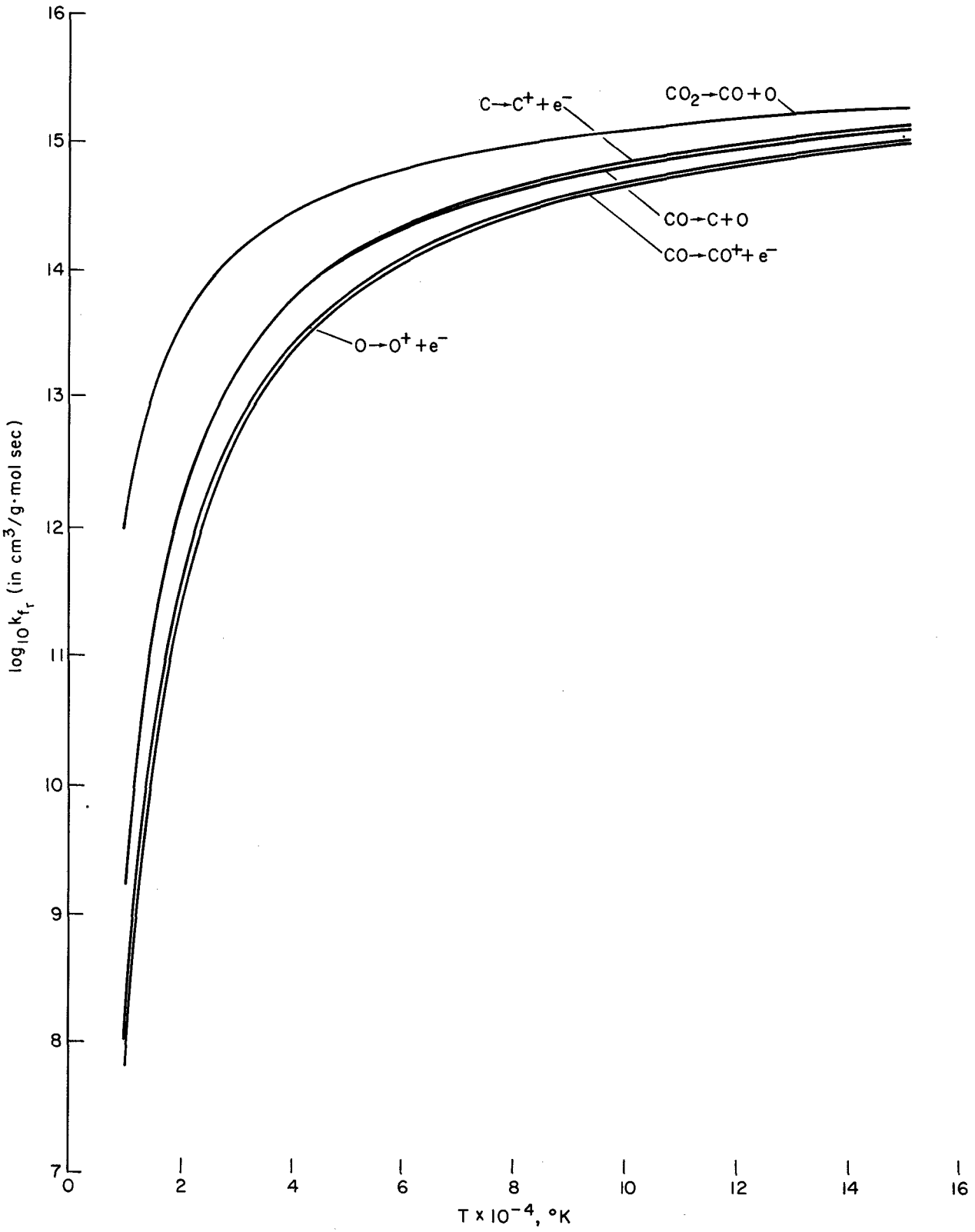

Figure 1.- Reaction rate coefficient estimates.

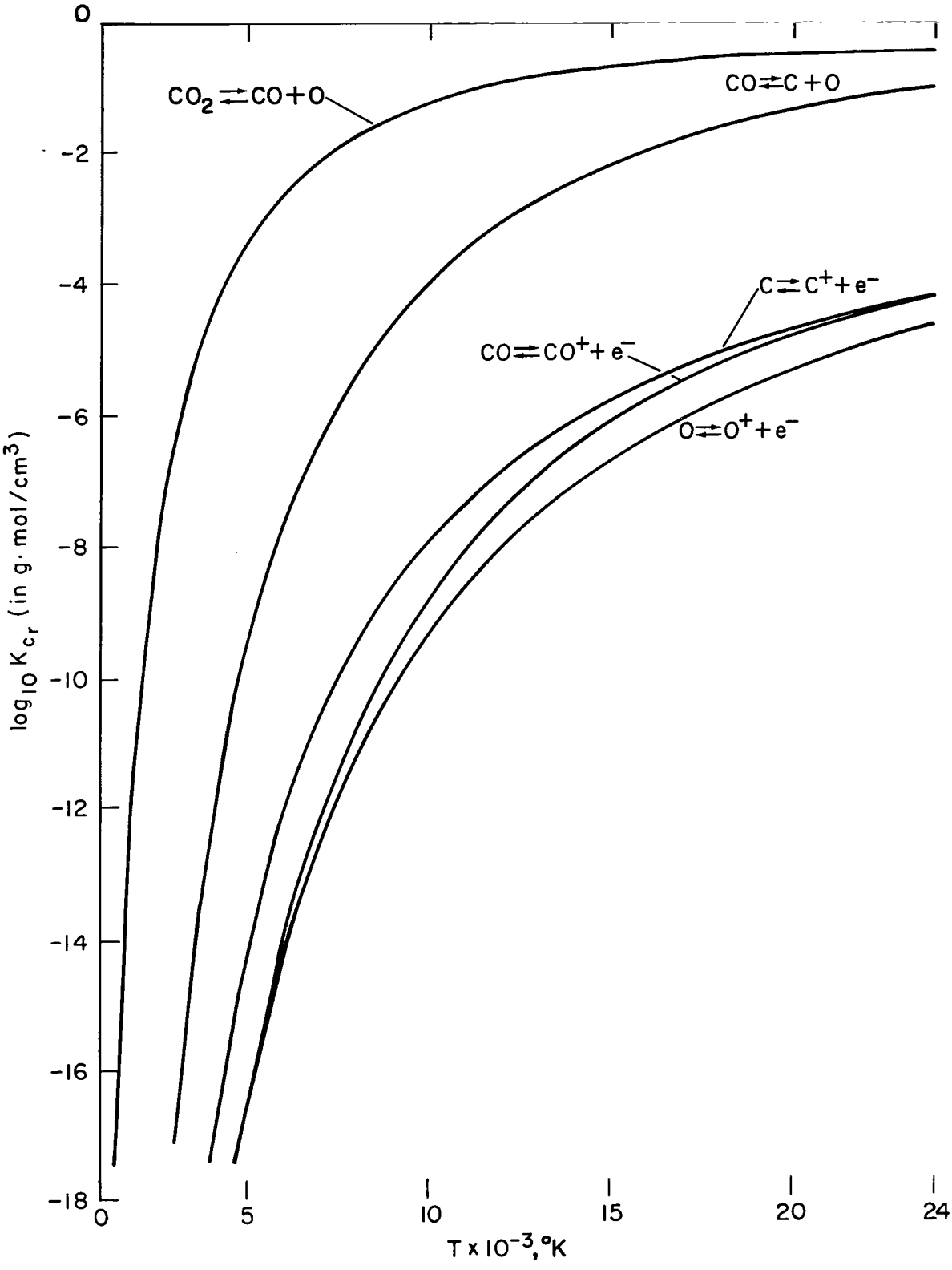

Figure 2.- Equilibrium coefficients.

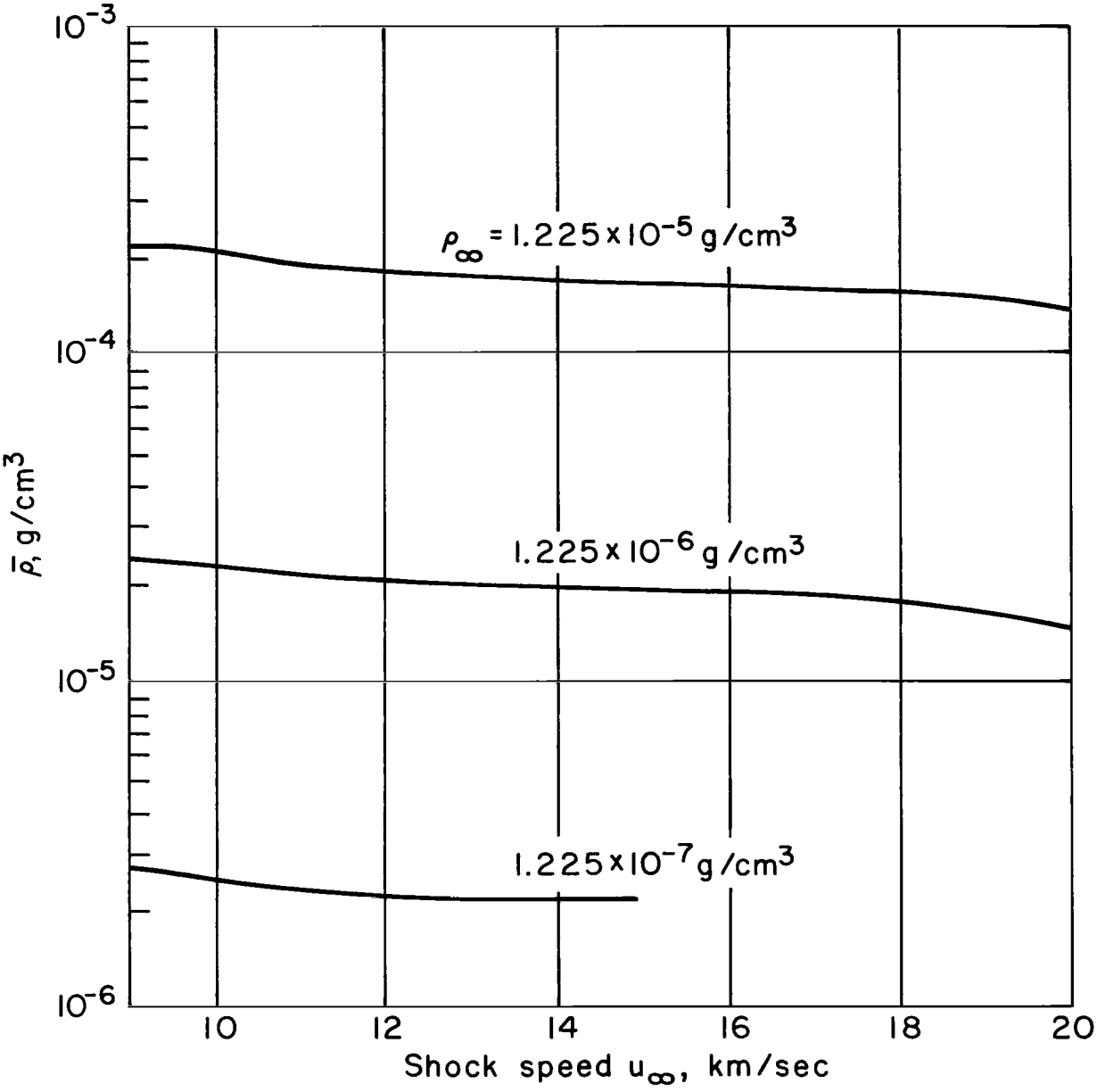

Figure 3.- Equilibrium density behind normal shock wave.

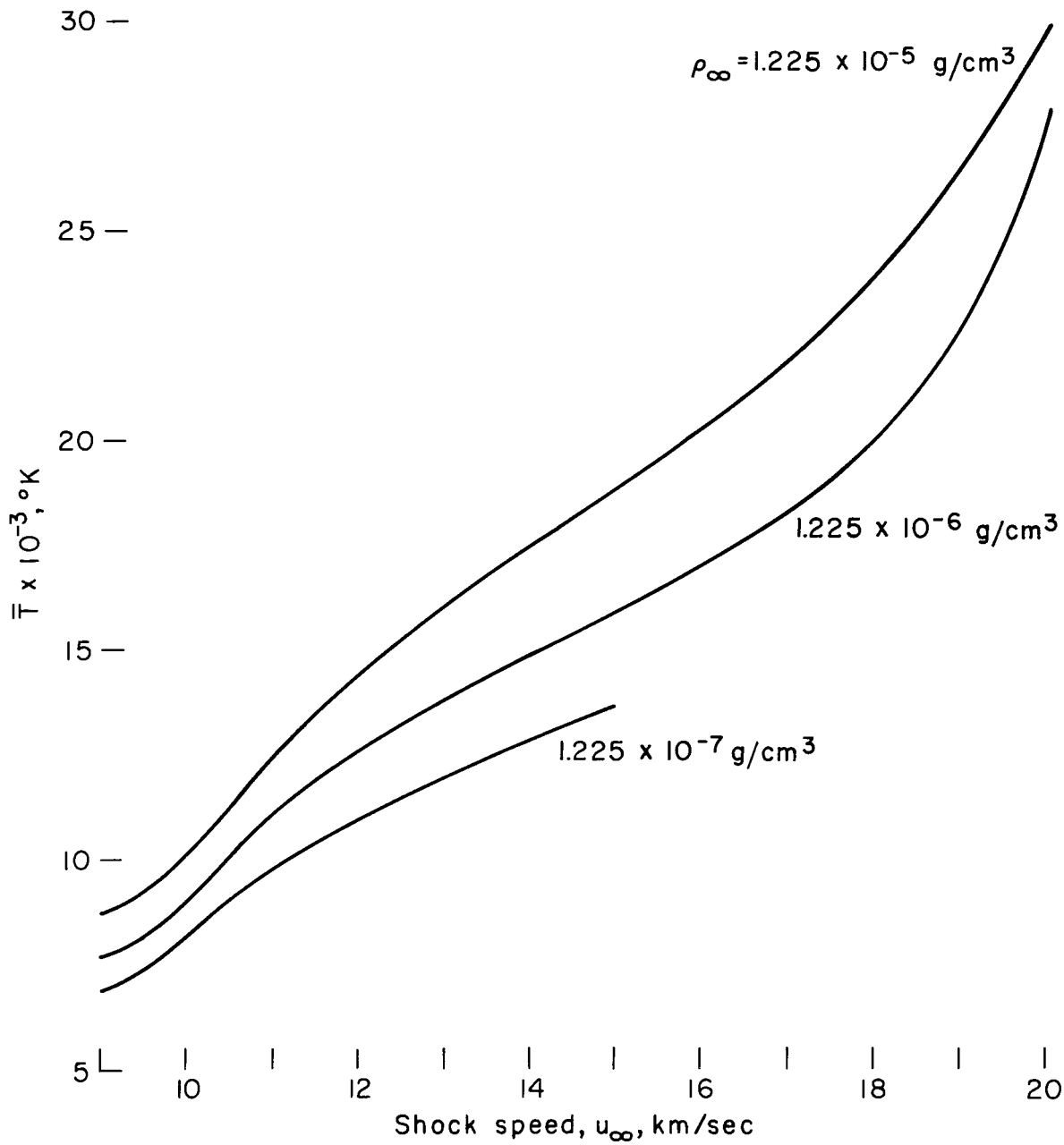

Figure 4.- Equilibrium temperature behind normal shock waves.

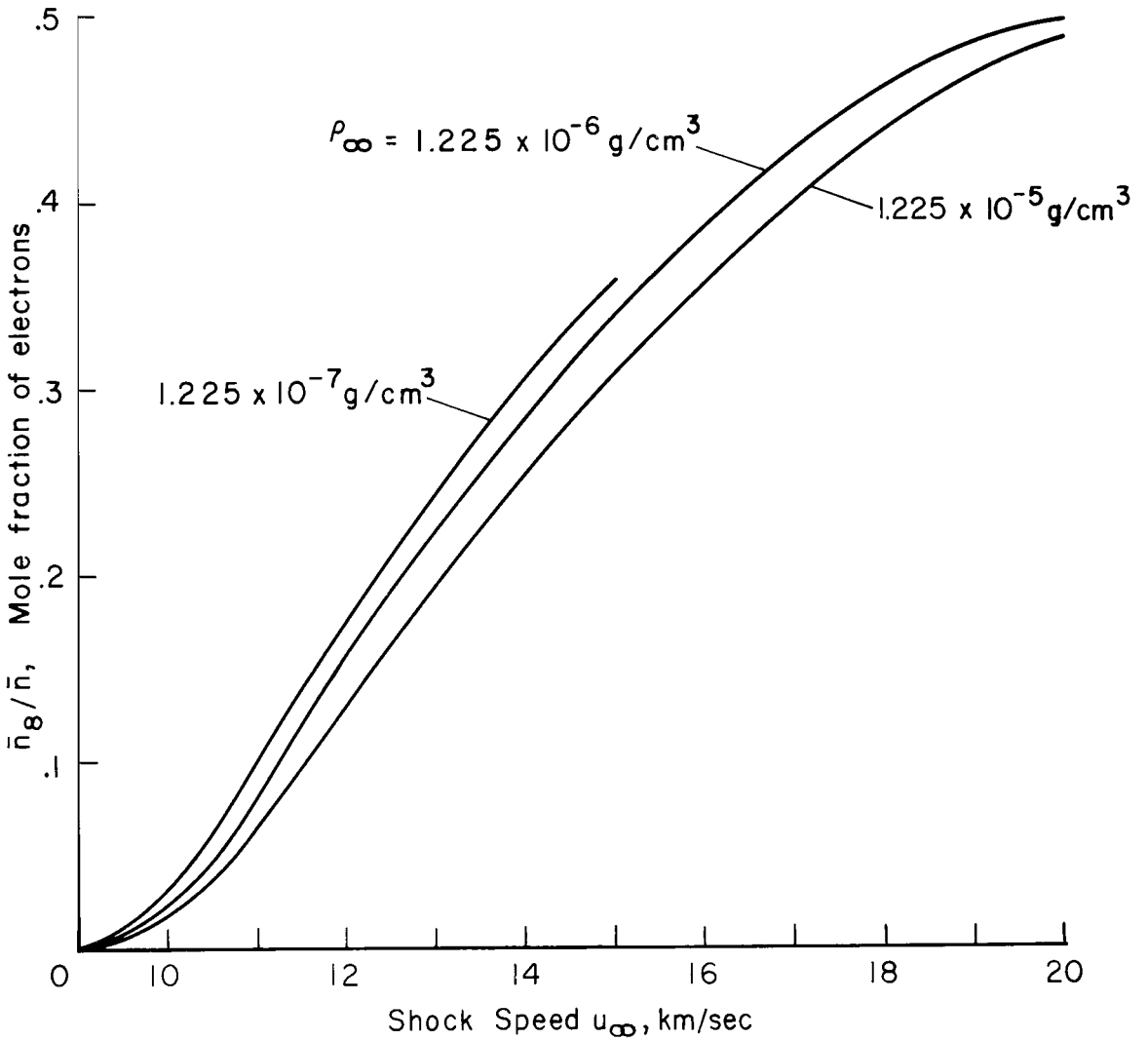

Figure 5.- Equilibrium electron concentration behind normal shock waves.

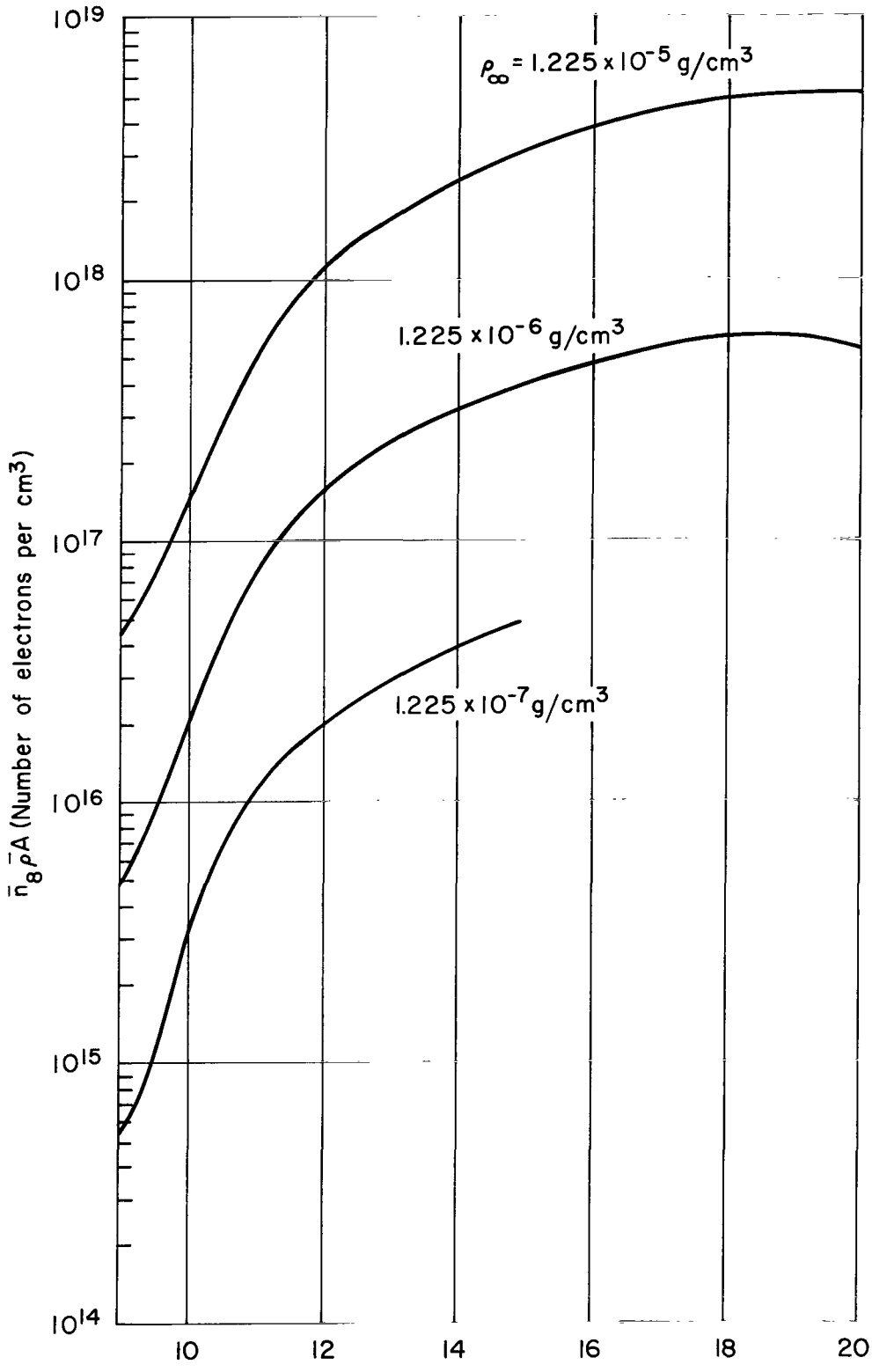

Figure 6.- Equilibrium electron density behind normal shock waves.

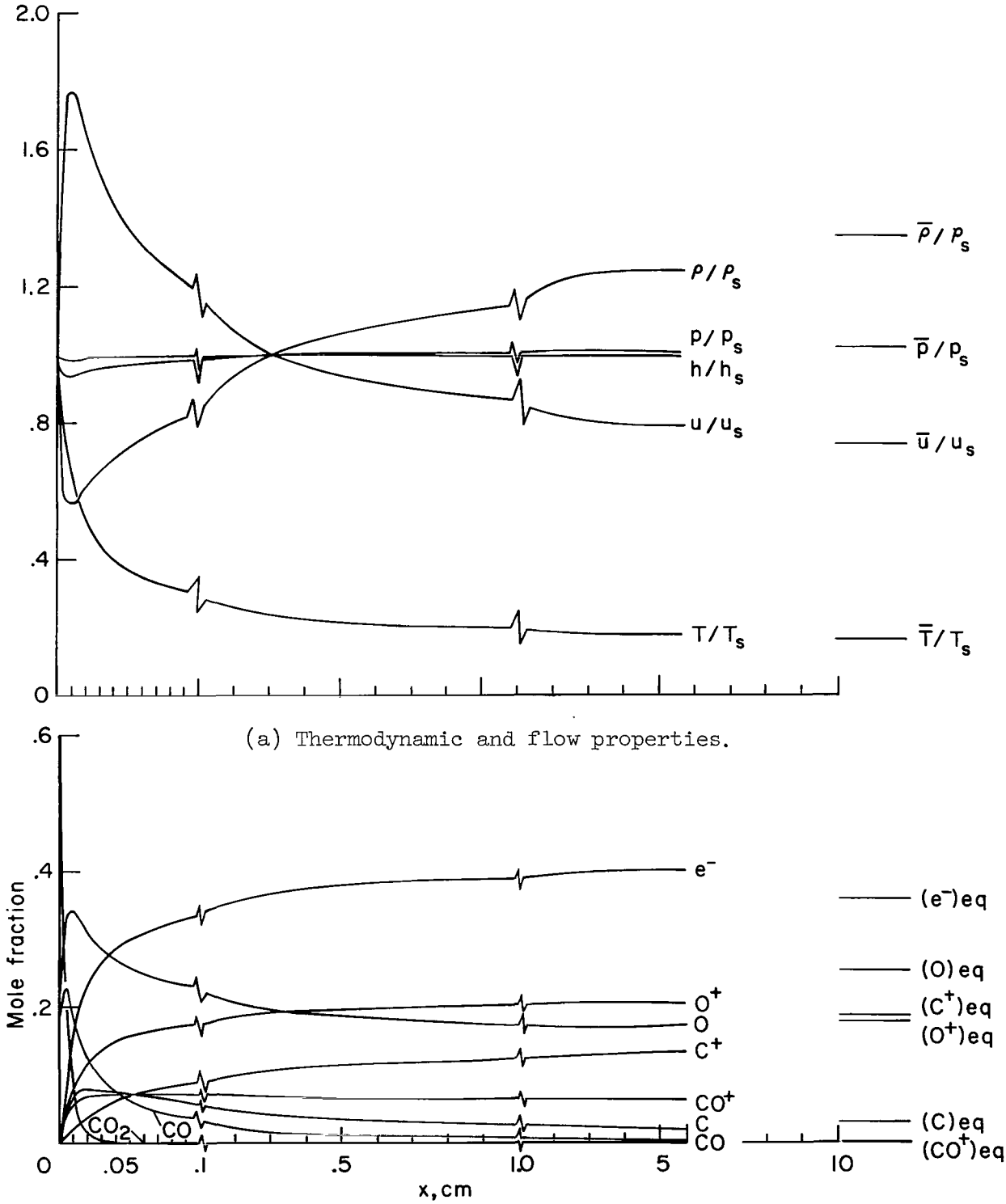

(a) Thermodynamic and flow properties.

(b) Species concentration.

Figure 7.- Nonequilibrium profiles; u_∞ = 15 km/sec, $\rho_\infty/\rho_o = 10^{-4}$.

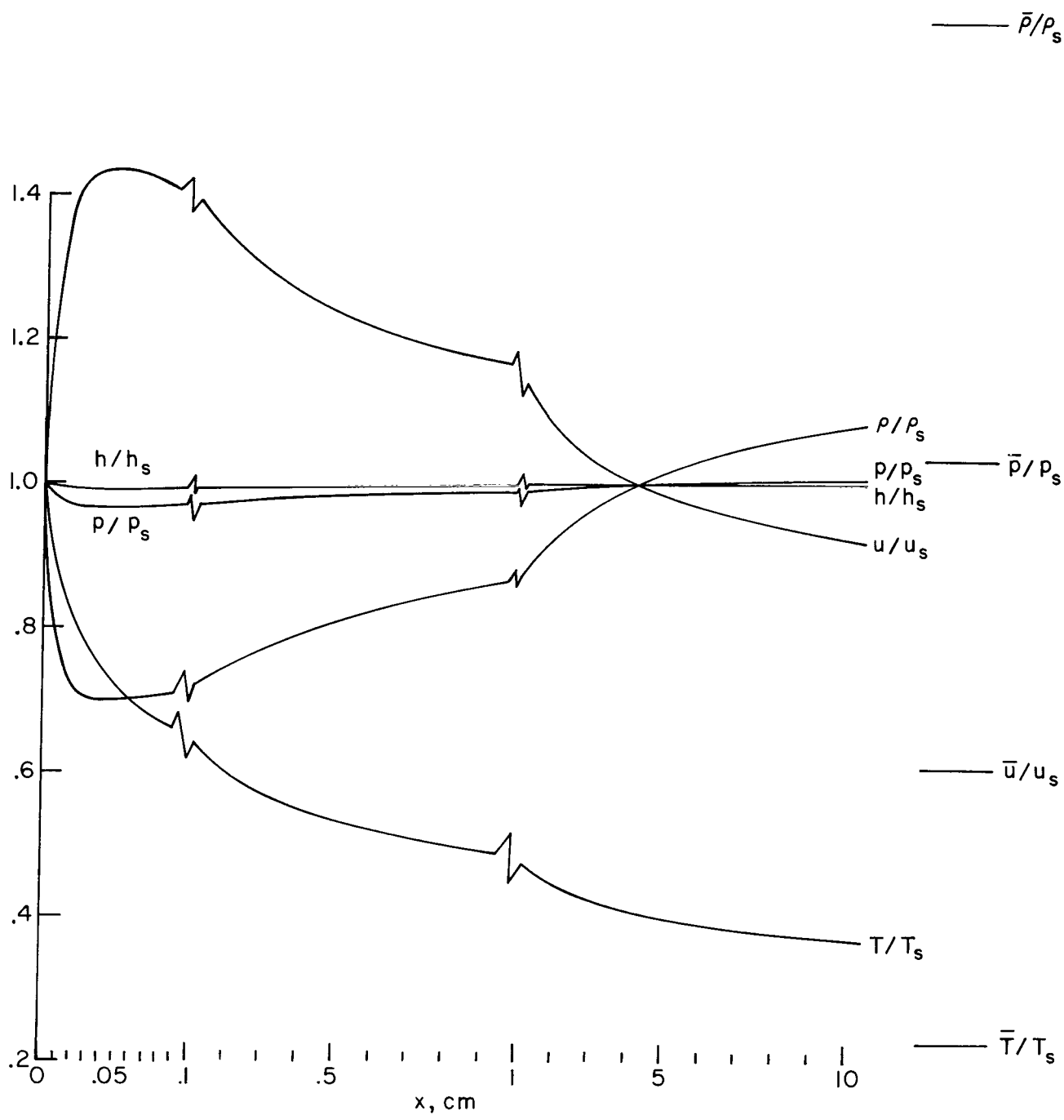

(a) Thermodynamic and flow properties.

Figure 8.- Nonequilibrium profiles; u_∞ = 9 km/sec, $\rho_\infty/\rho_o = 10^{-4}$.

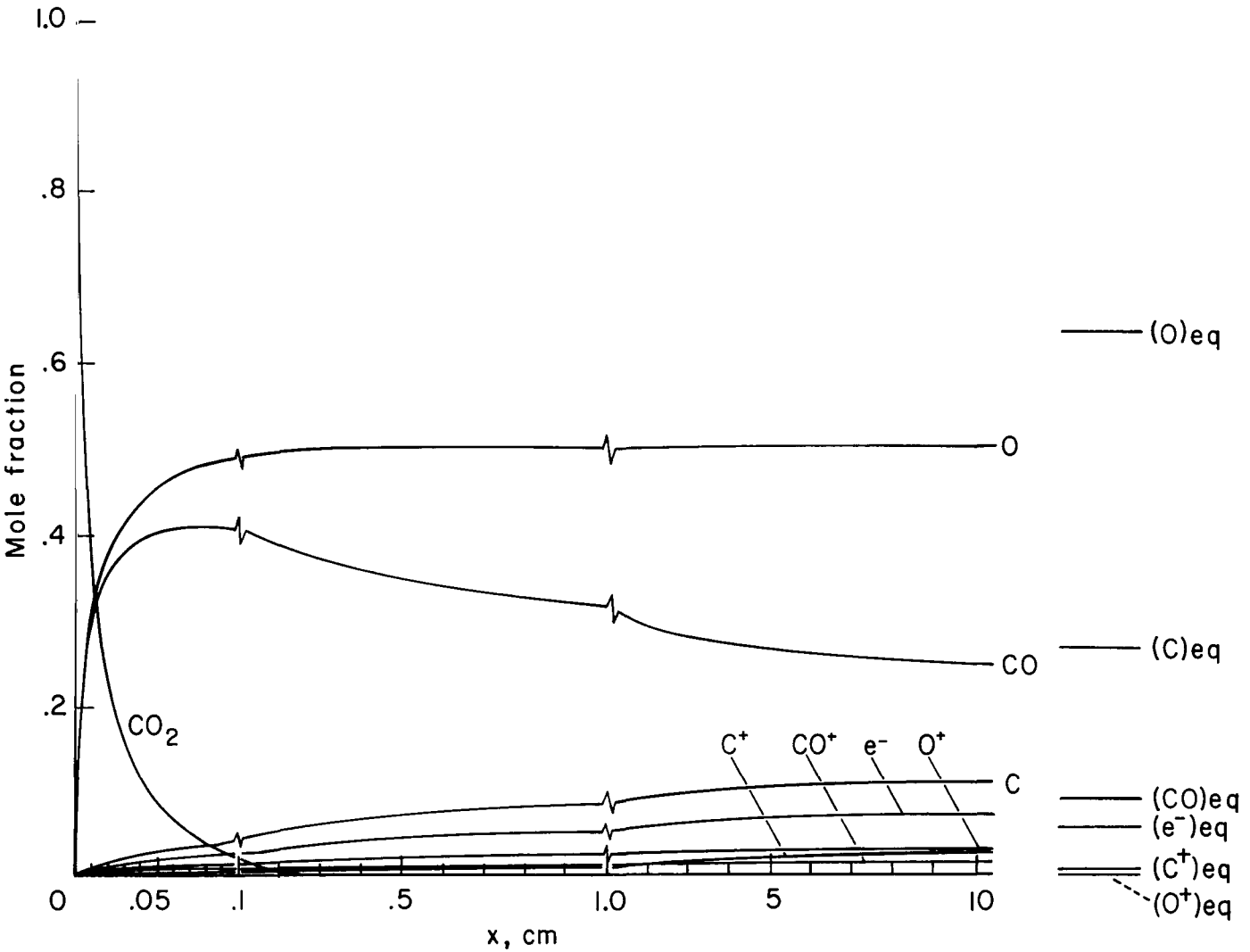

(b) Species concentration.

Figure 8.- Concluded.

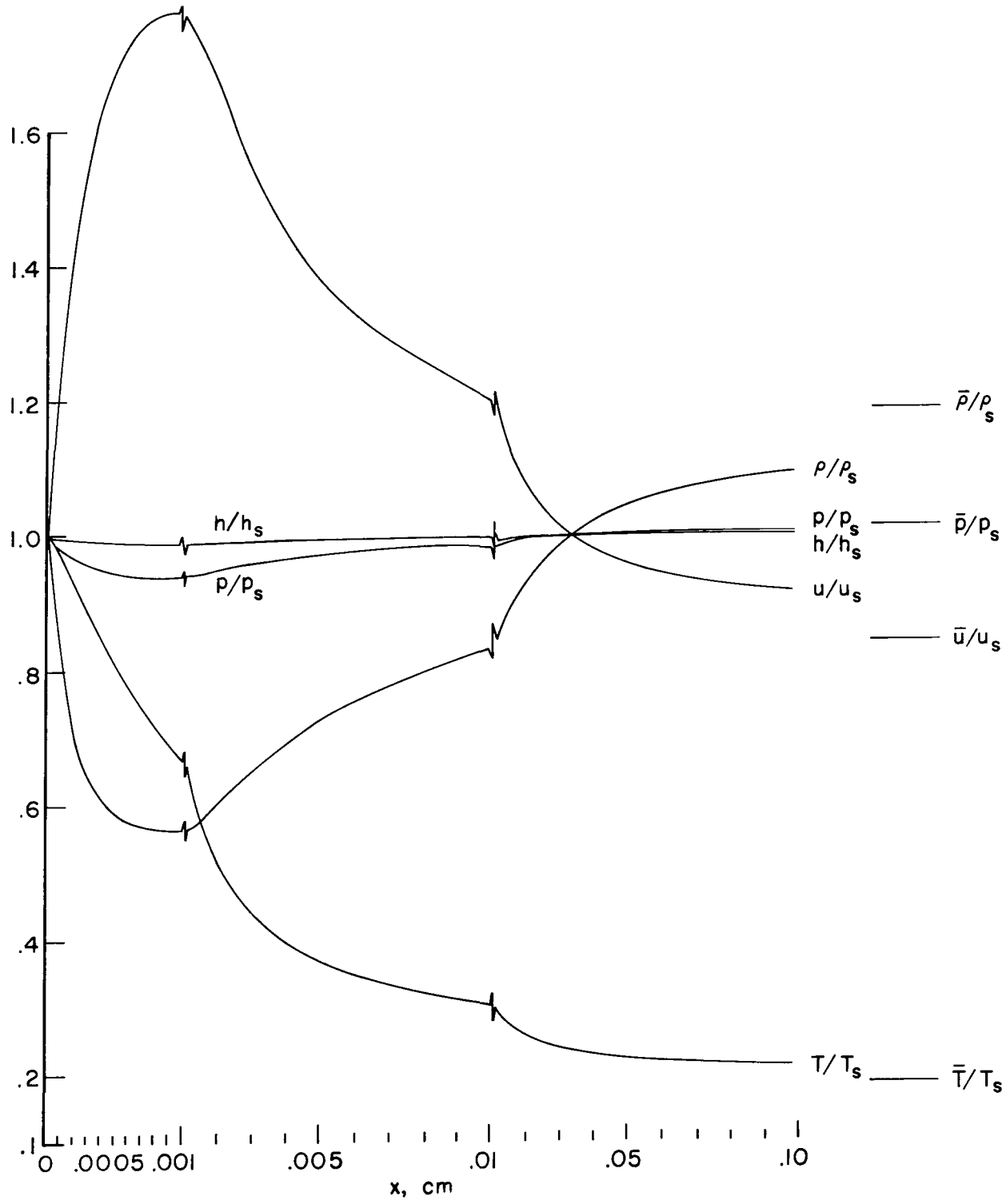

(a) Thermodynamic and flow properties.

Figure 9.- Nonequilibrium profiles; u_∞ = 15 km/sec, $\rho_\infty/\rho_O = 10^{-3}$.

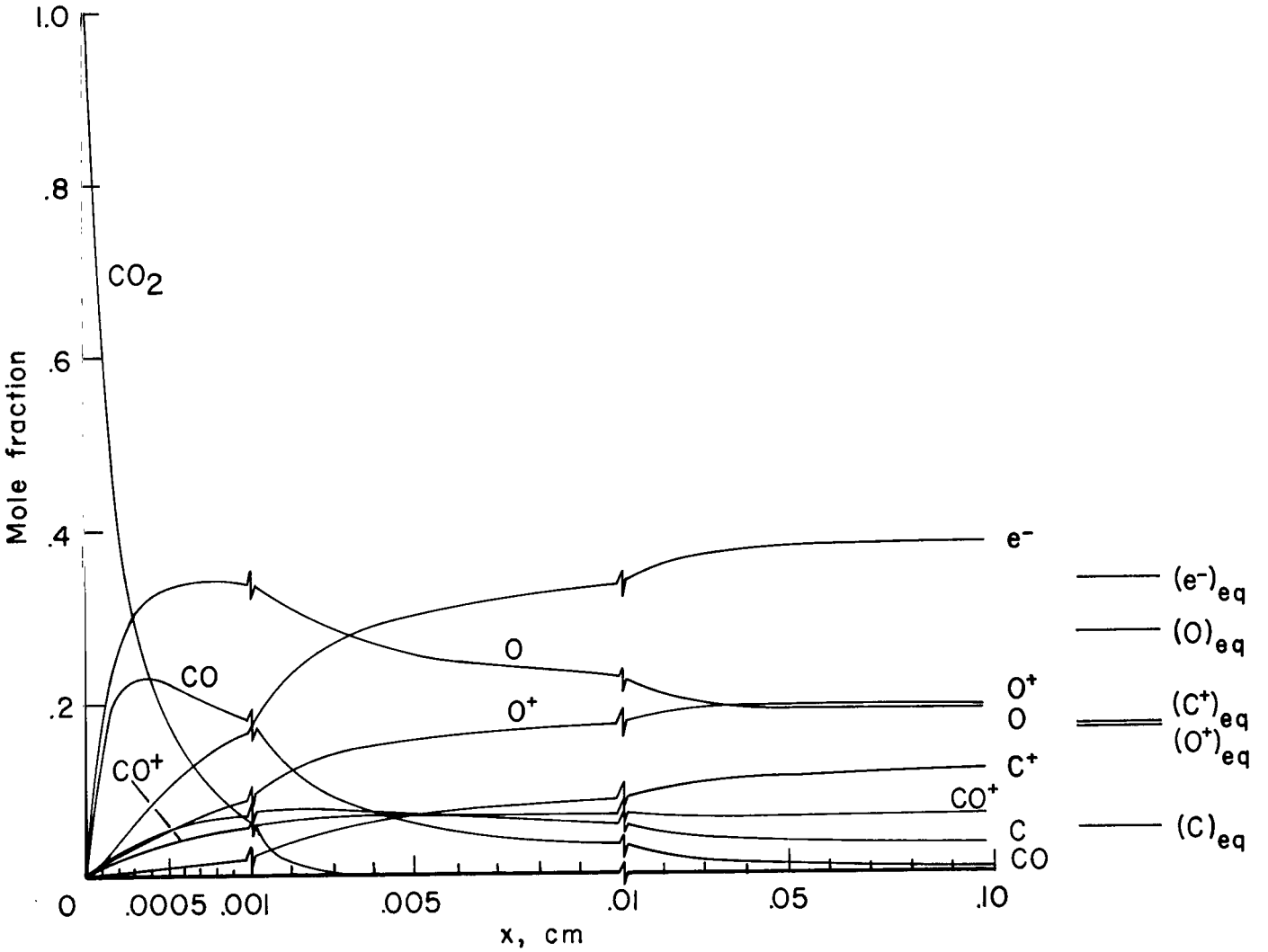

(b) Species concentration.

Figure 9.- Concluded.

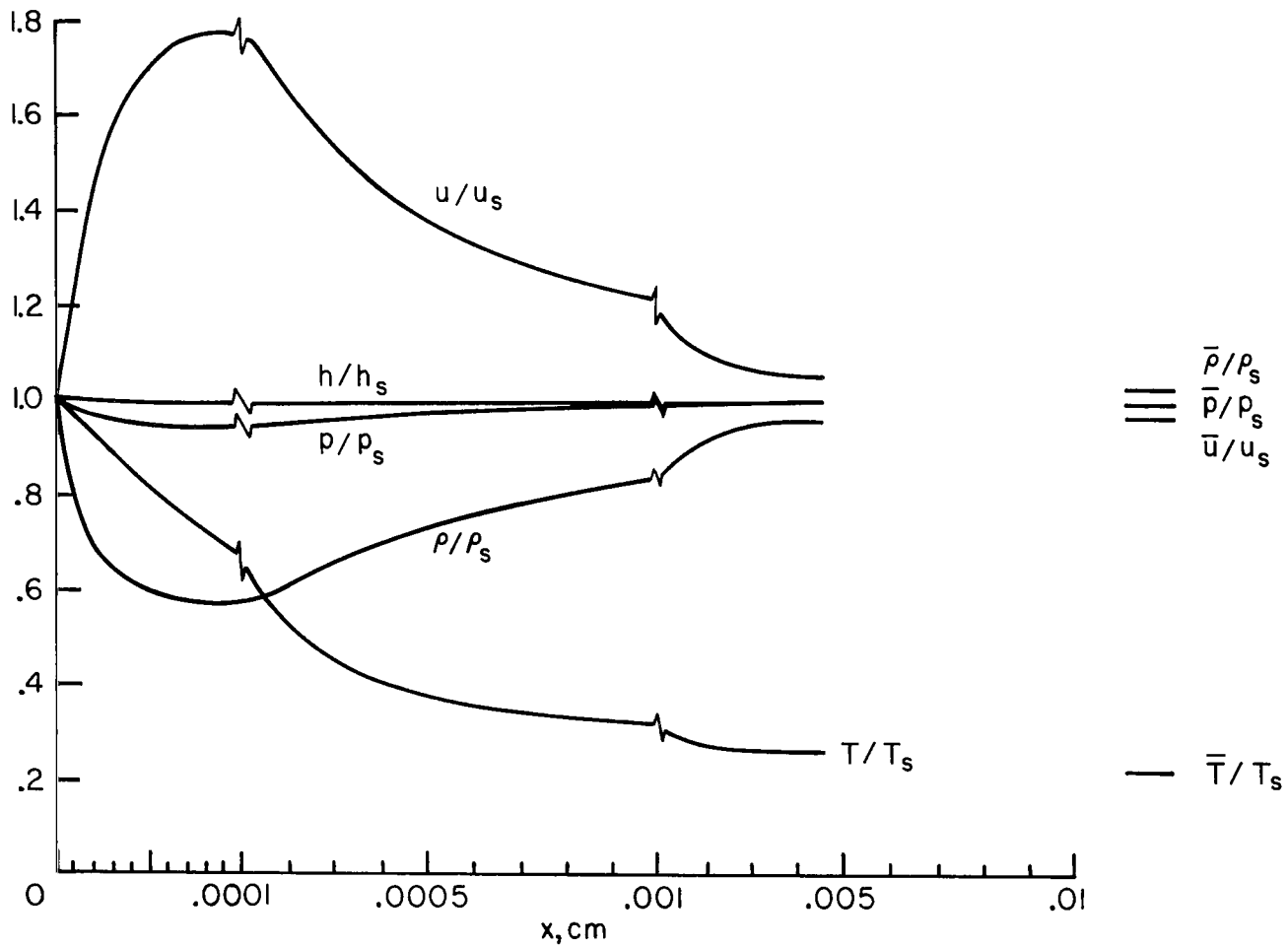

(a) Thermodynamic and flow properties.

Figure 10.- Nonequilibrium profiles; u_∞ = 15 km/sec, $\rho_\infty/\rho_o = 10^{-2}$.

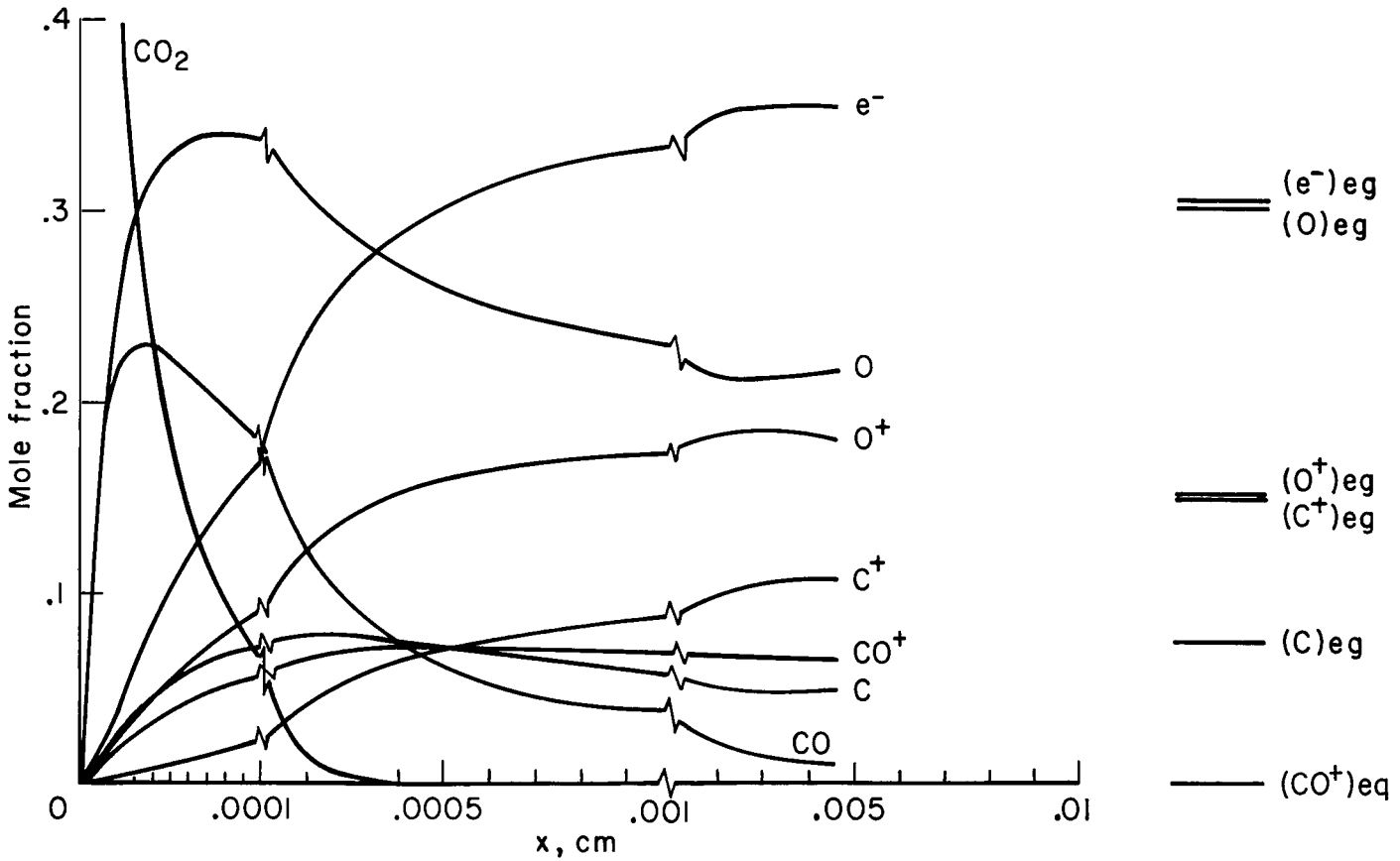

(b) Species concentration.

Figure 10.- Concluded.

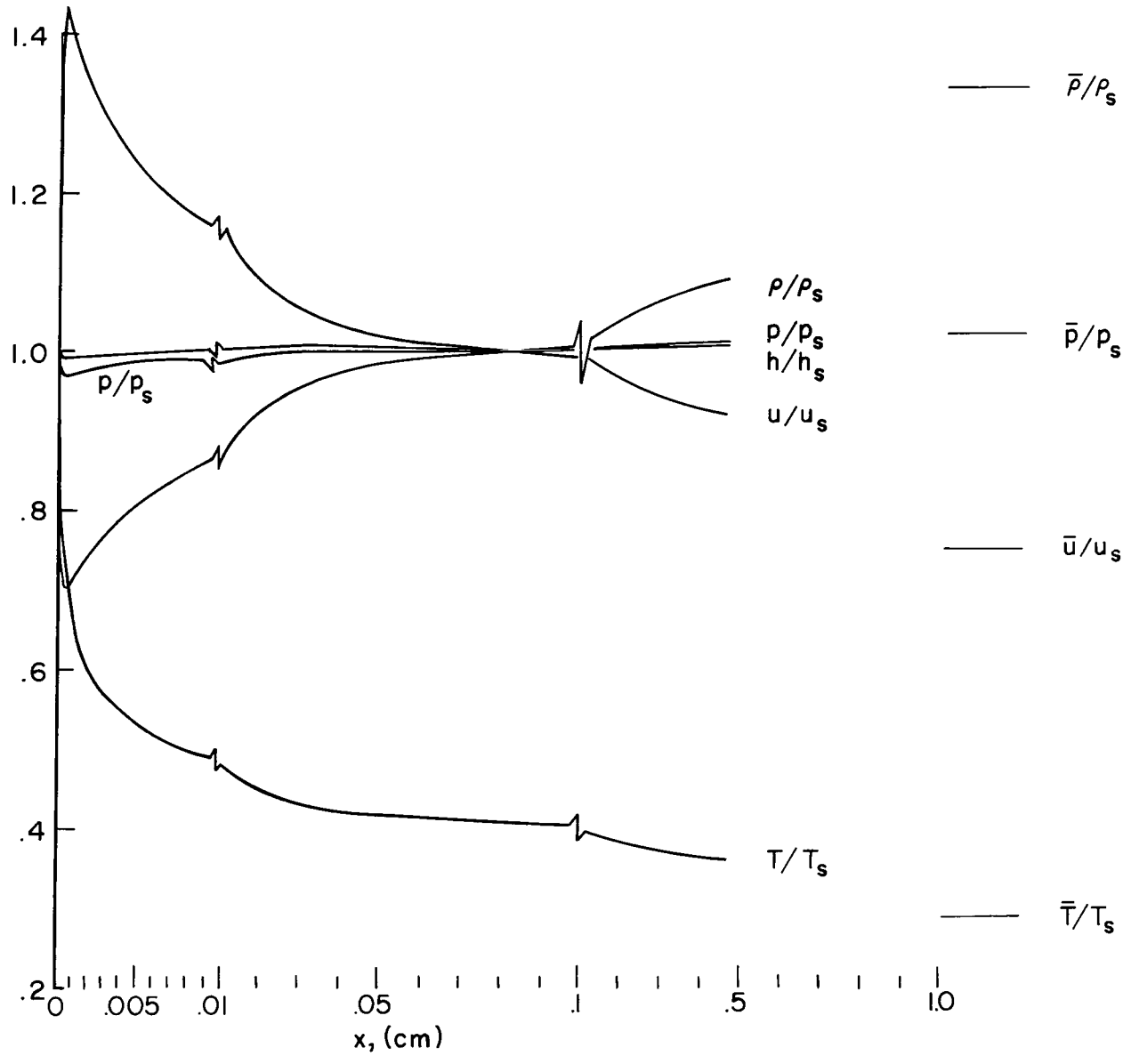

(a) Thermodynamic and flow properties.

Figure 11.- Nonequilibrium profiles; u_∞ = 9 km/sec, $\rho_\infty/\rho_0 = 10^{-2}$.

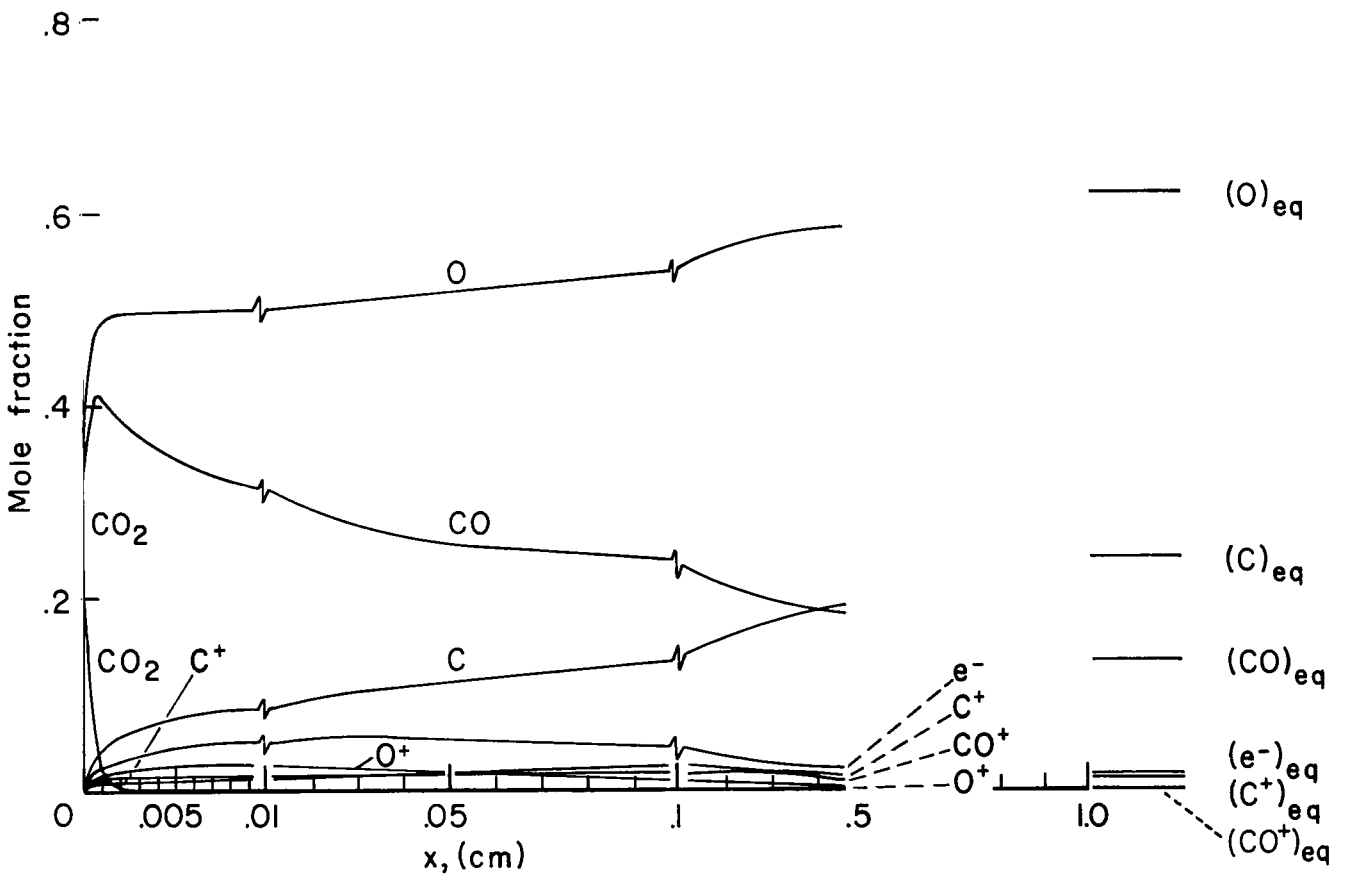

(b) Species concentration.

Figure 11.- Concluded.

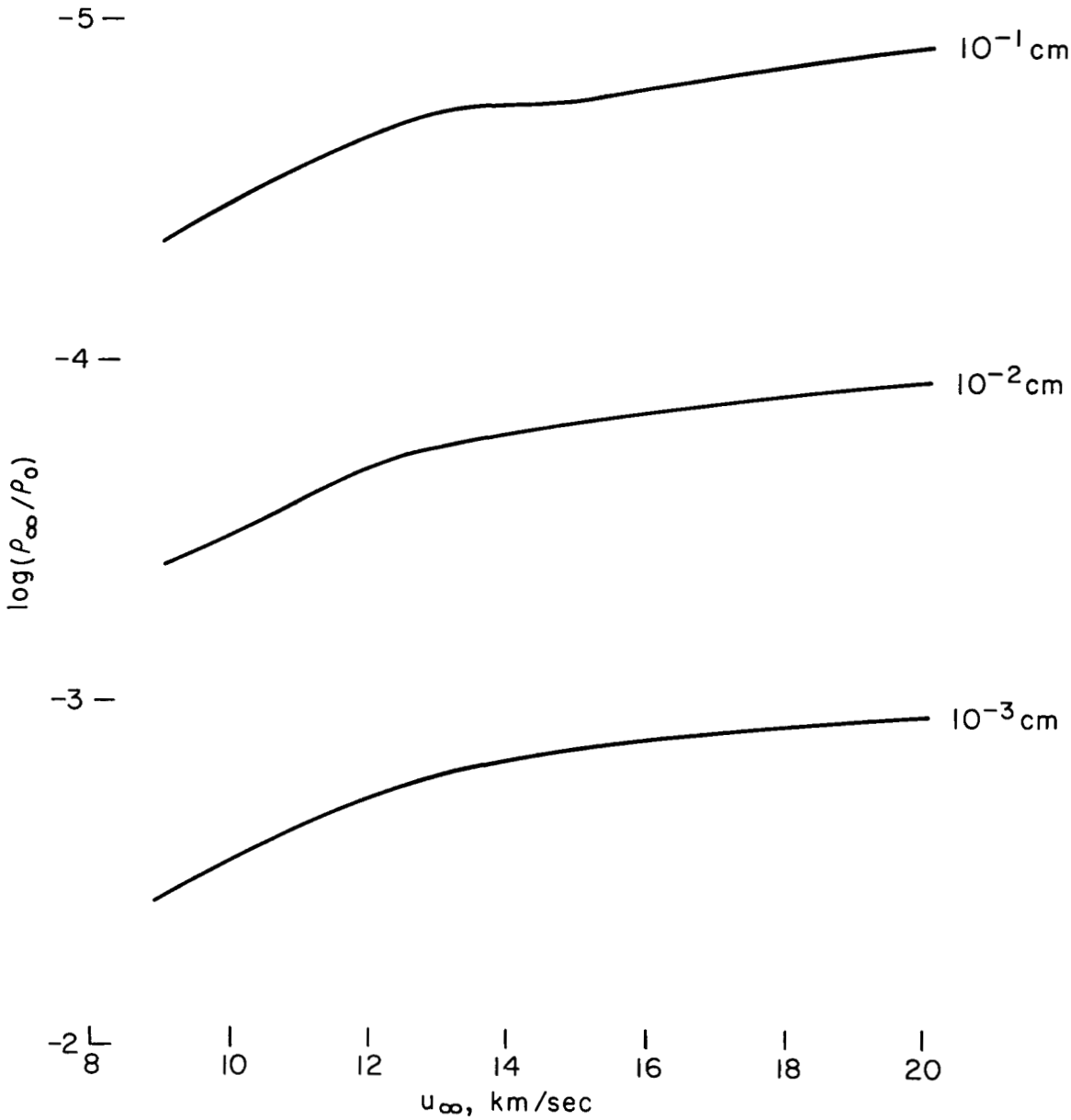

Figure 12.- Relaxation distance for 50-percent reaction completion.

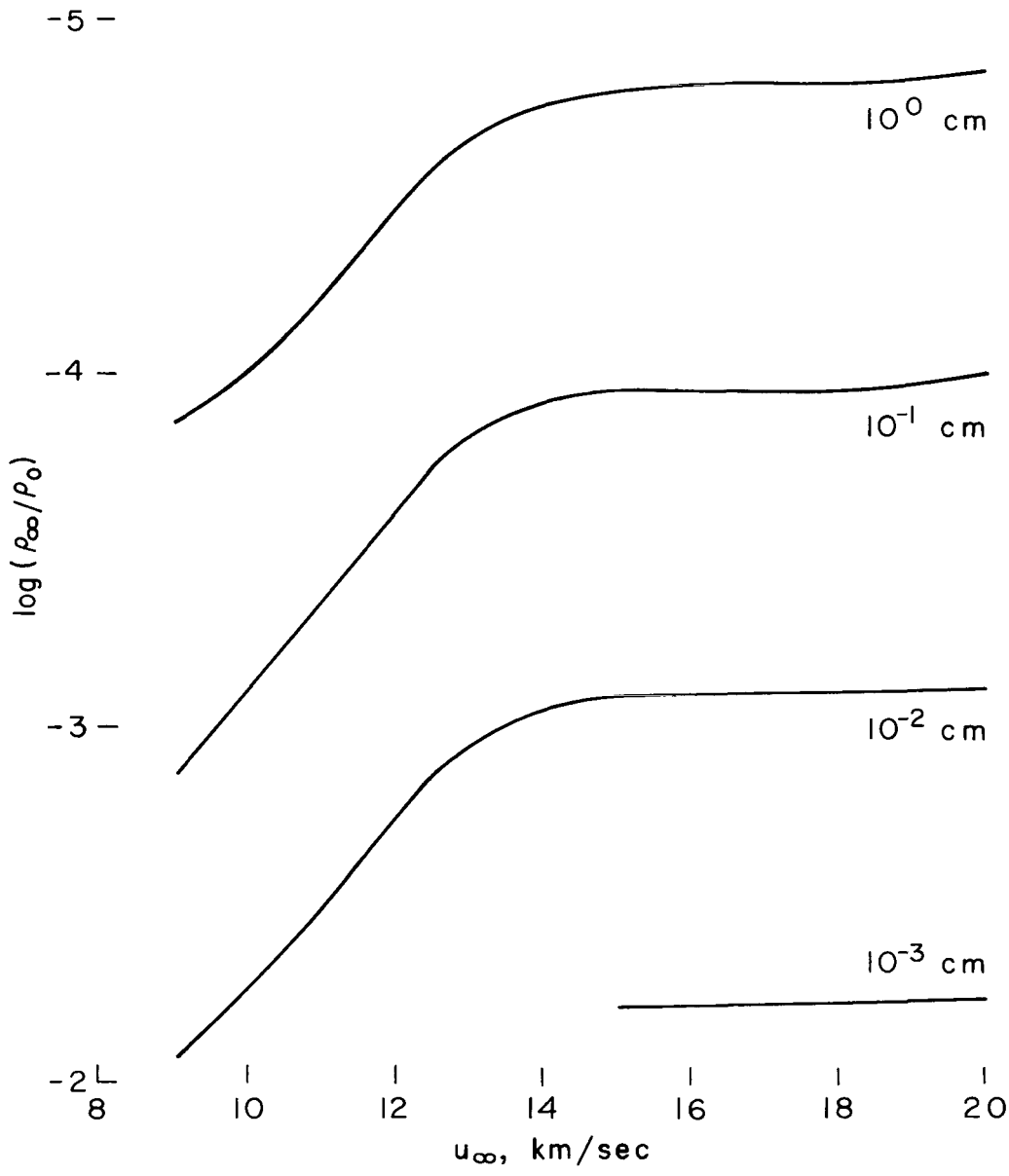

Figure 13.- Relaxation distance for 80-percent reaction completion.

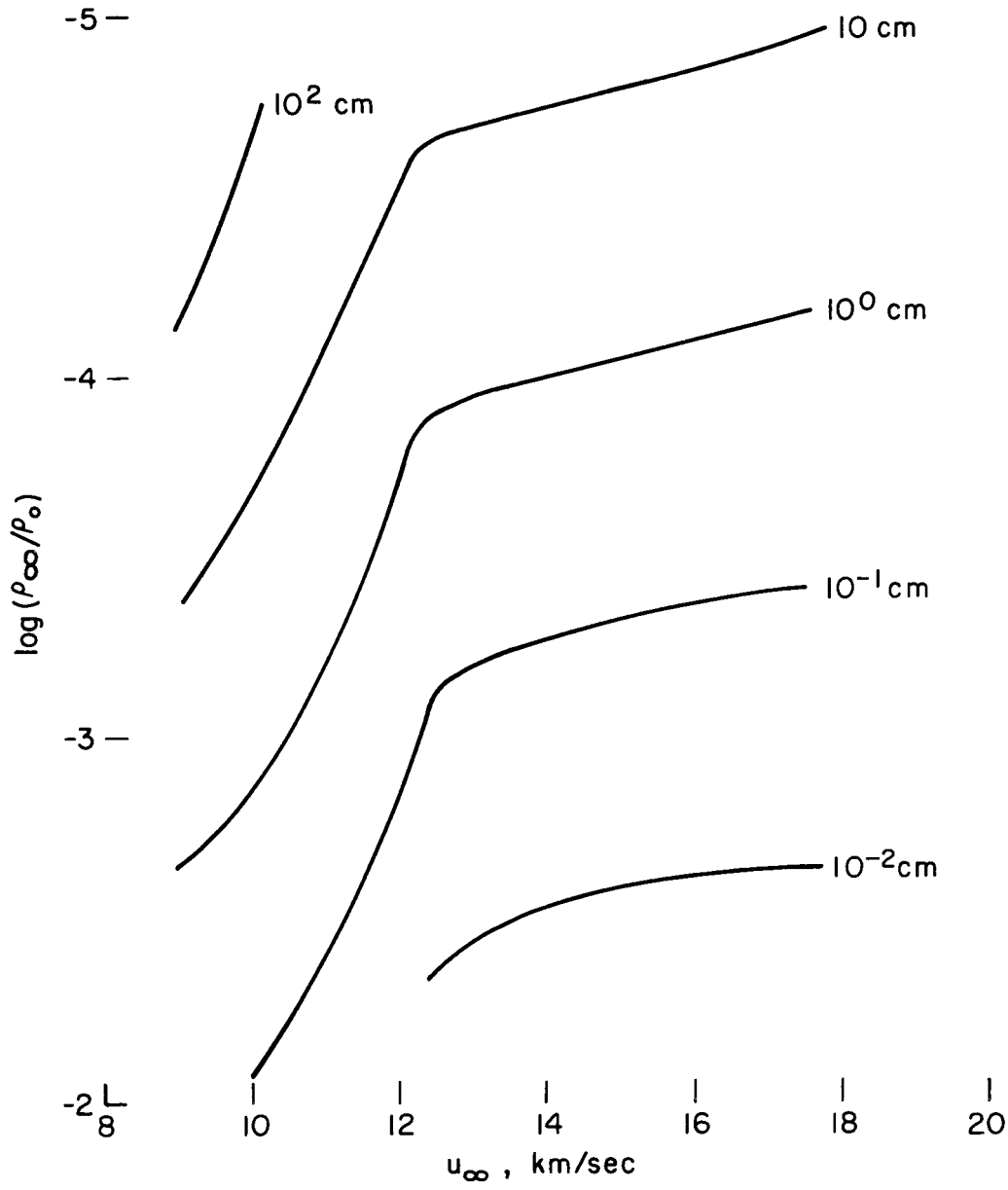

Figure 14.- Relaxation distance for 90-percent reaction completion.

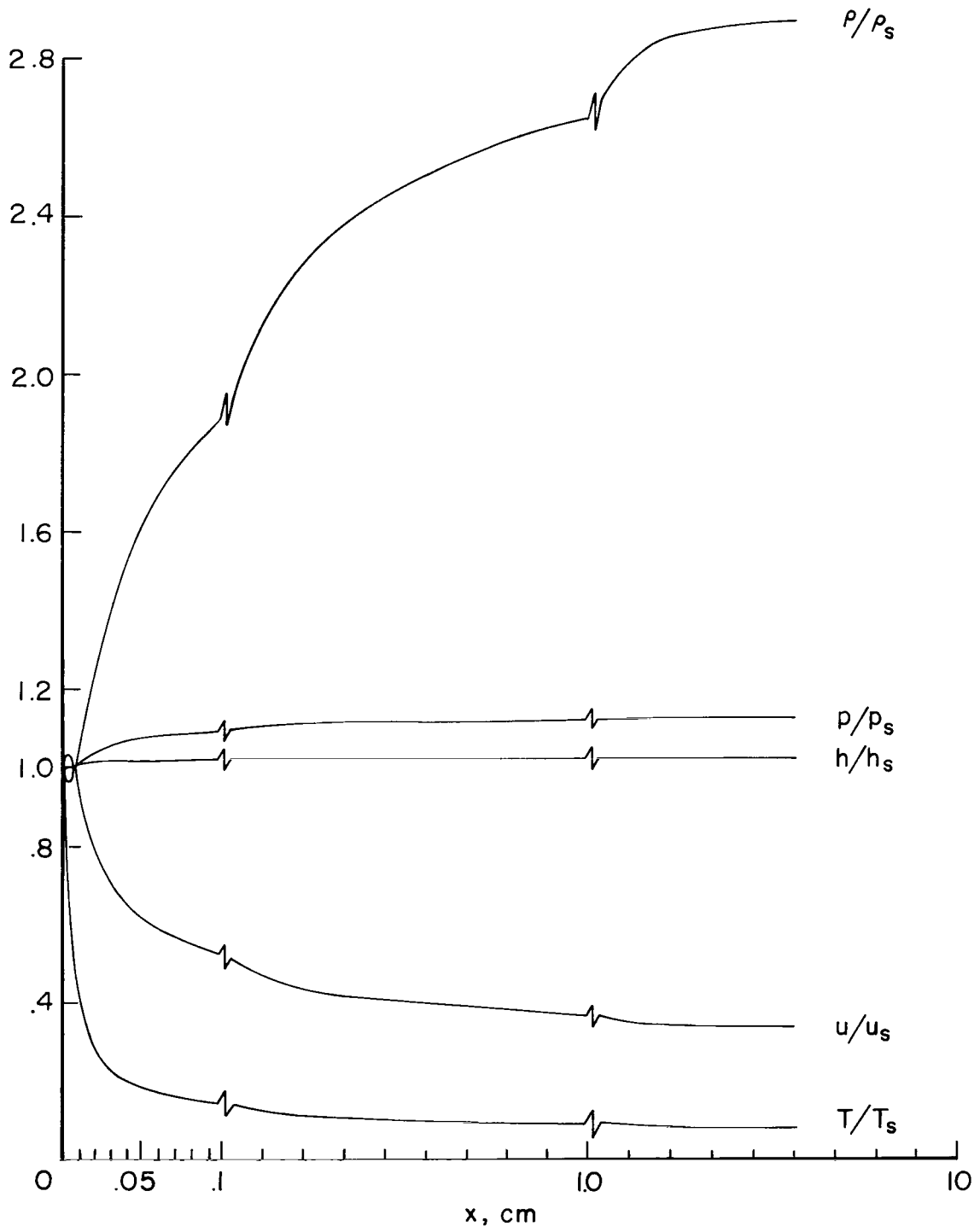

(a) Thermodynamic and flow properties.

Figure 15.- Nonequilibrium profiles without vibrational excitation; u_∞ = 15 km/sec, $\rho_\infty/\rho_o = 10^{-4}$.

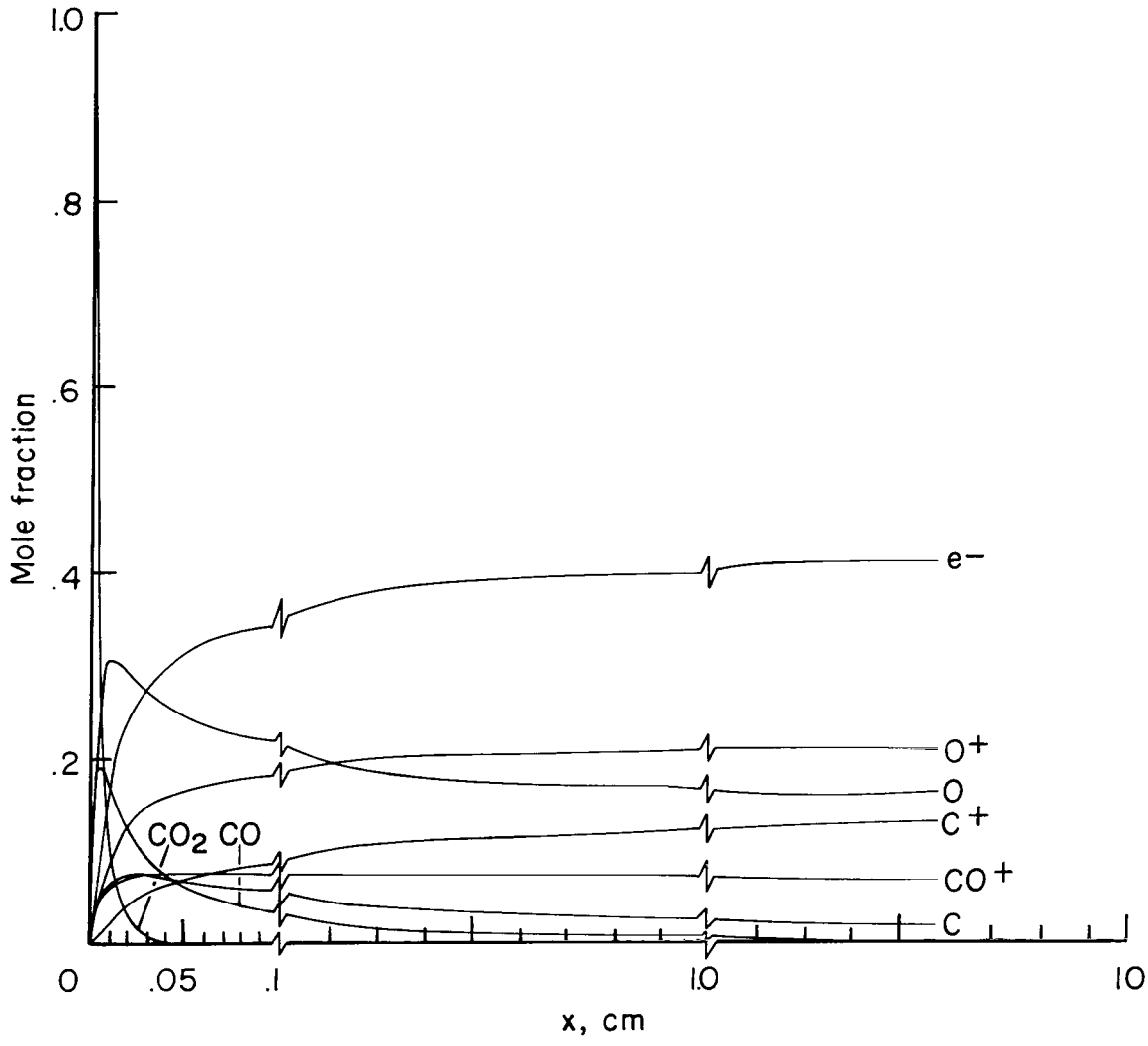

(b) Species concentration.

Figure 15.- Concluded.

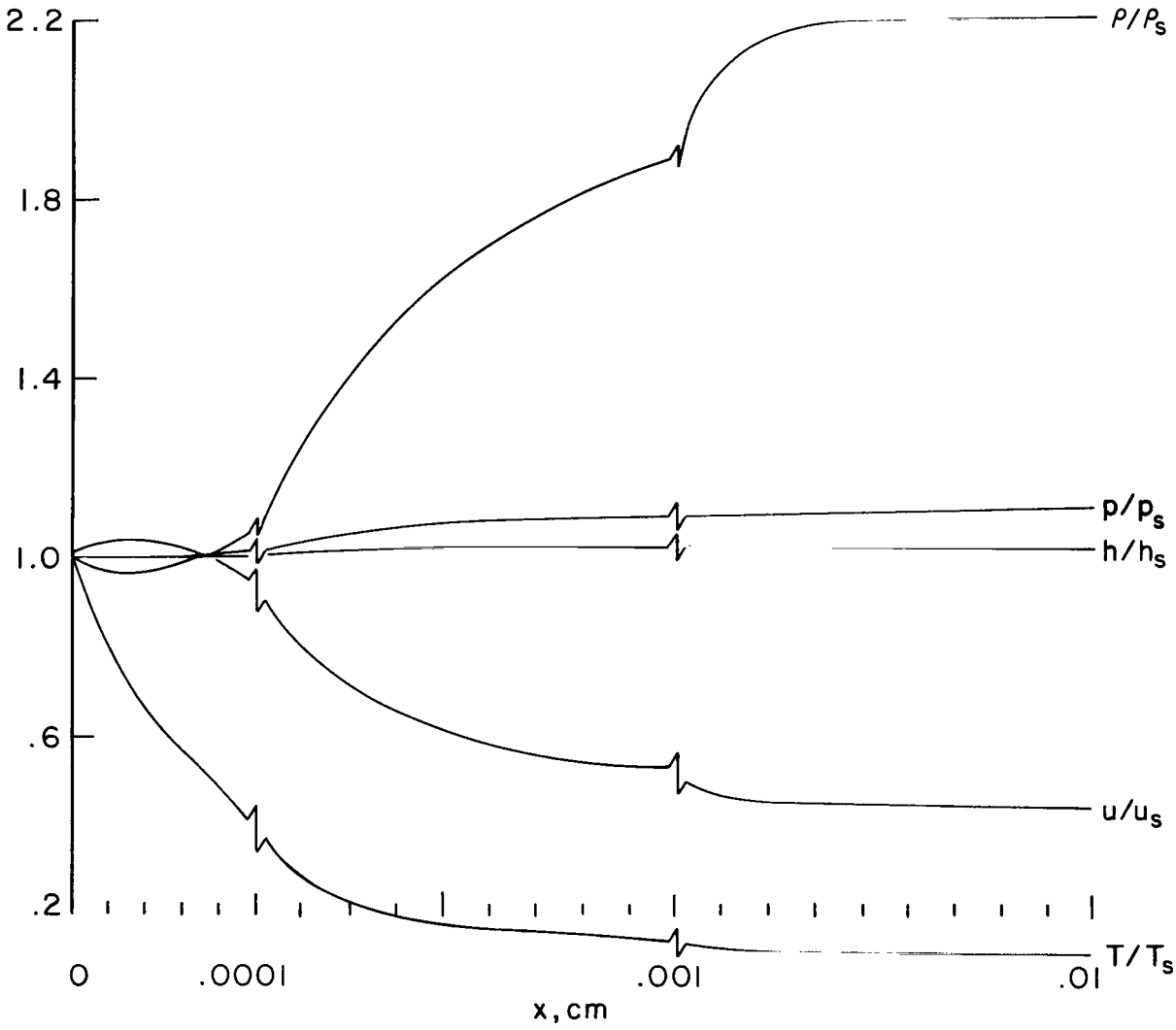

(a) Thermodynamic and flow properties.

Figure 16.- Nonequilibrium profiles without vibrational excitation; u_∞ = 15 km/sec, $\rho_\infty/\rho_O = 10^{-2}$.

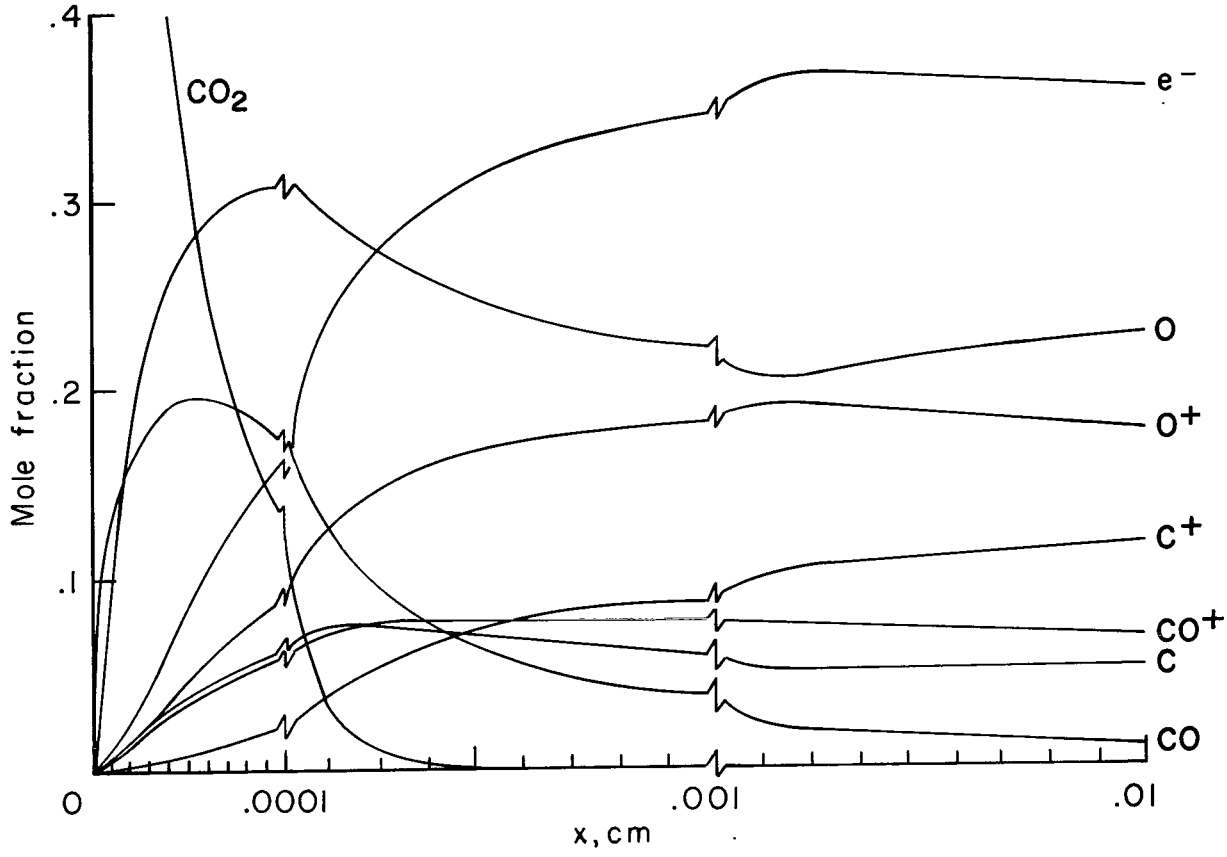

(b) Species concentration.

Figure 16.- Concluded.

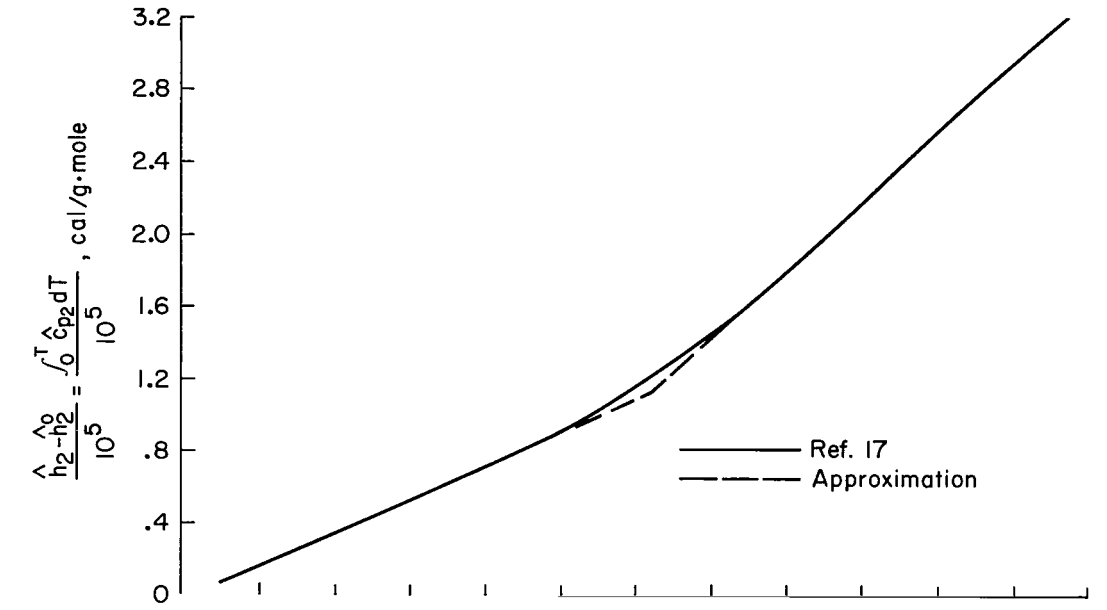

(a) Carbon monoxide.

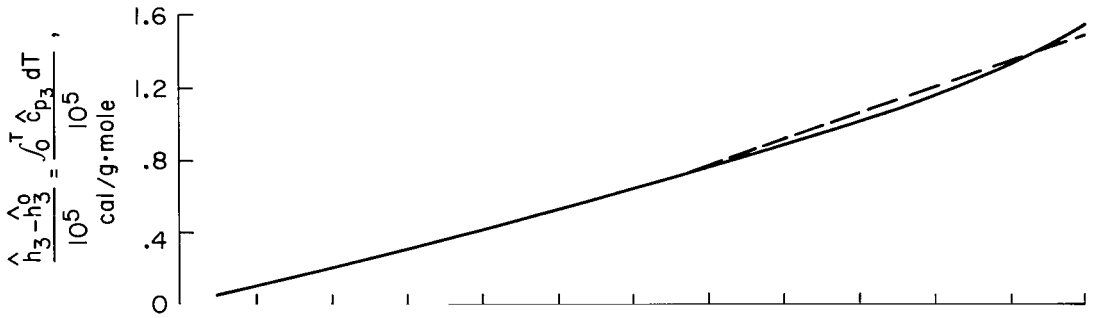

(b) Atomic oxygen.

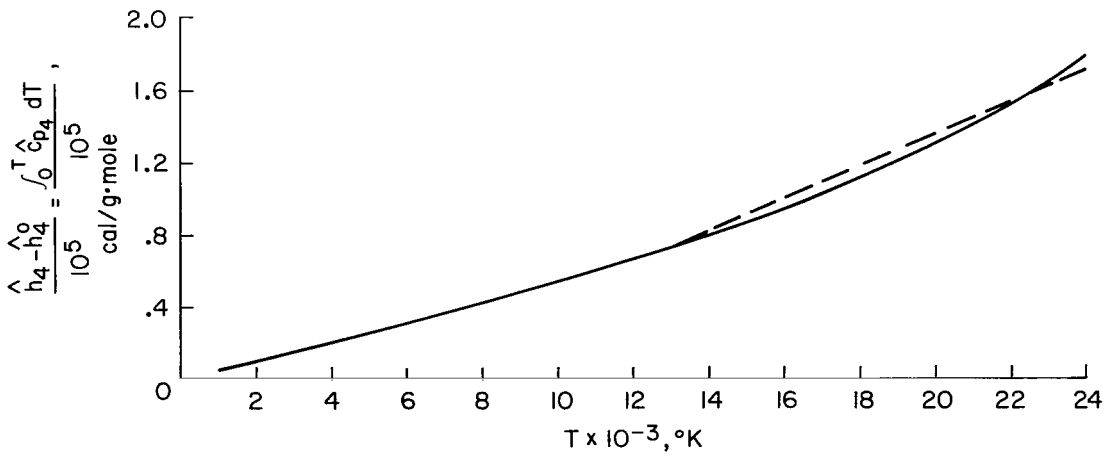

(c) Atomic carbon.

Figure 17.- Species enthalpy.

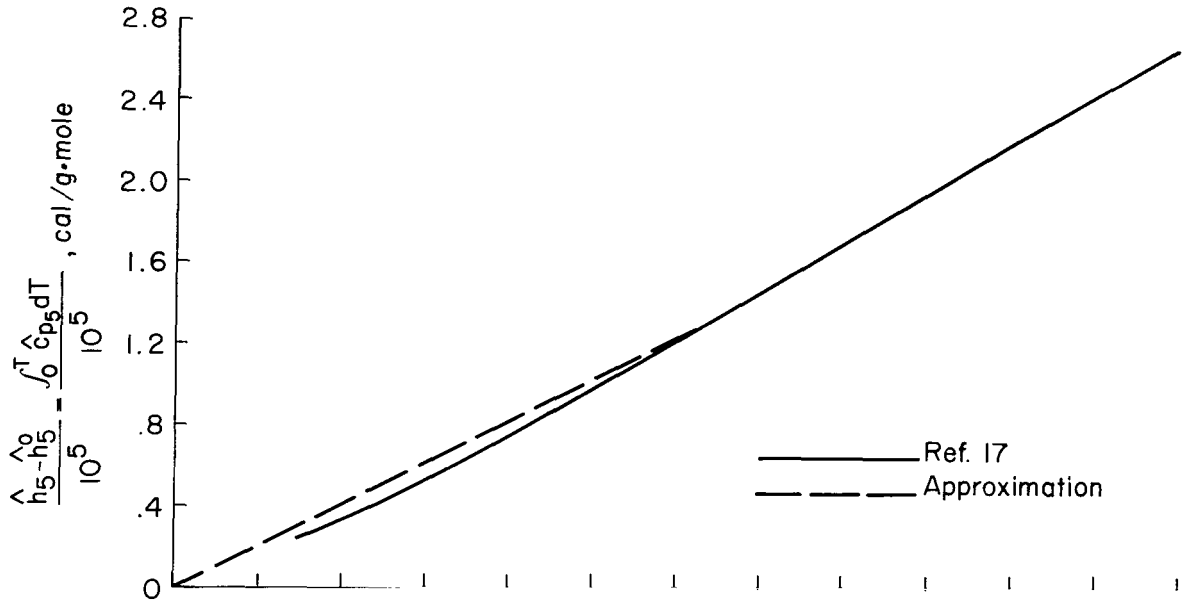

(d) Carbon monoxide ion.

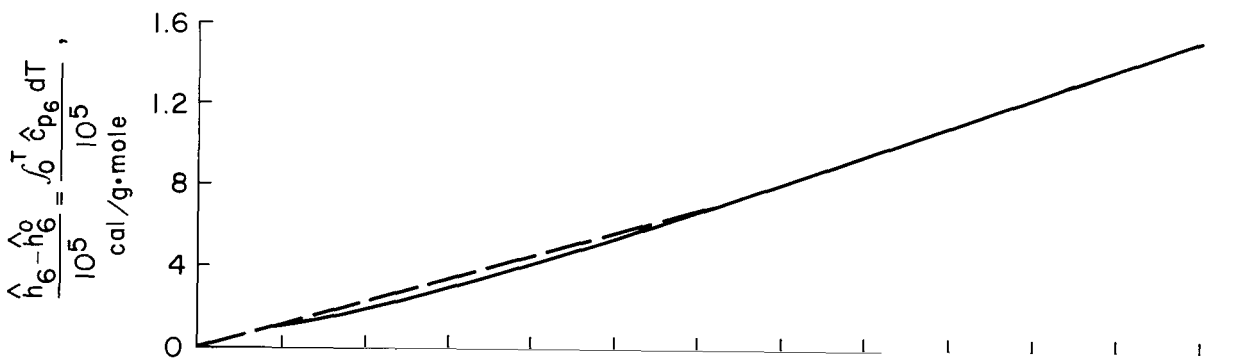

(e) Atomic oxygen ion.

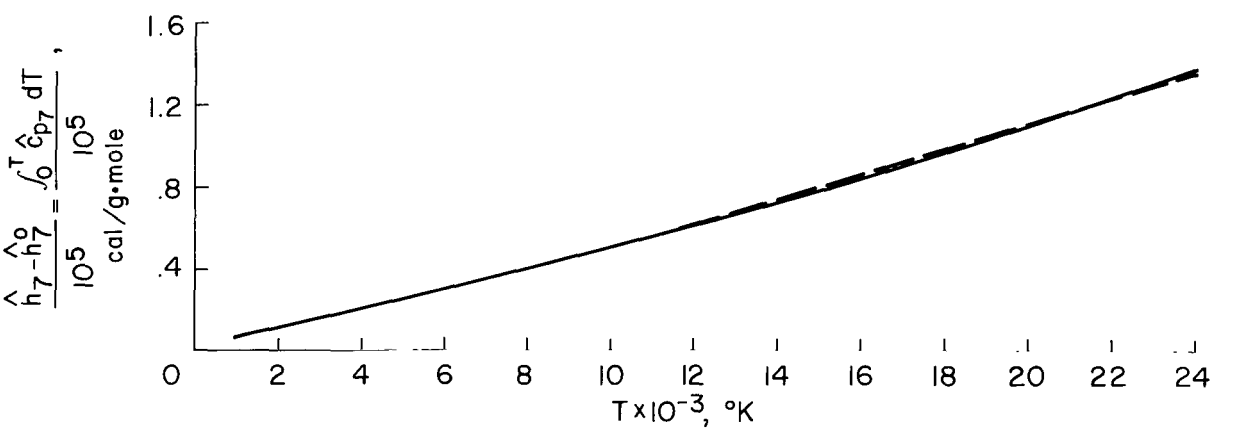

(f) Atomic carbon ion.

Figure 17.- Concluded.

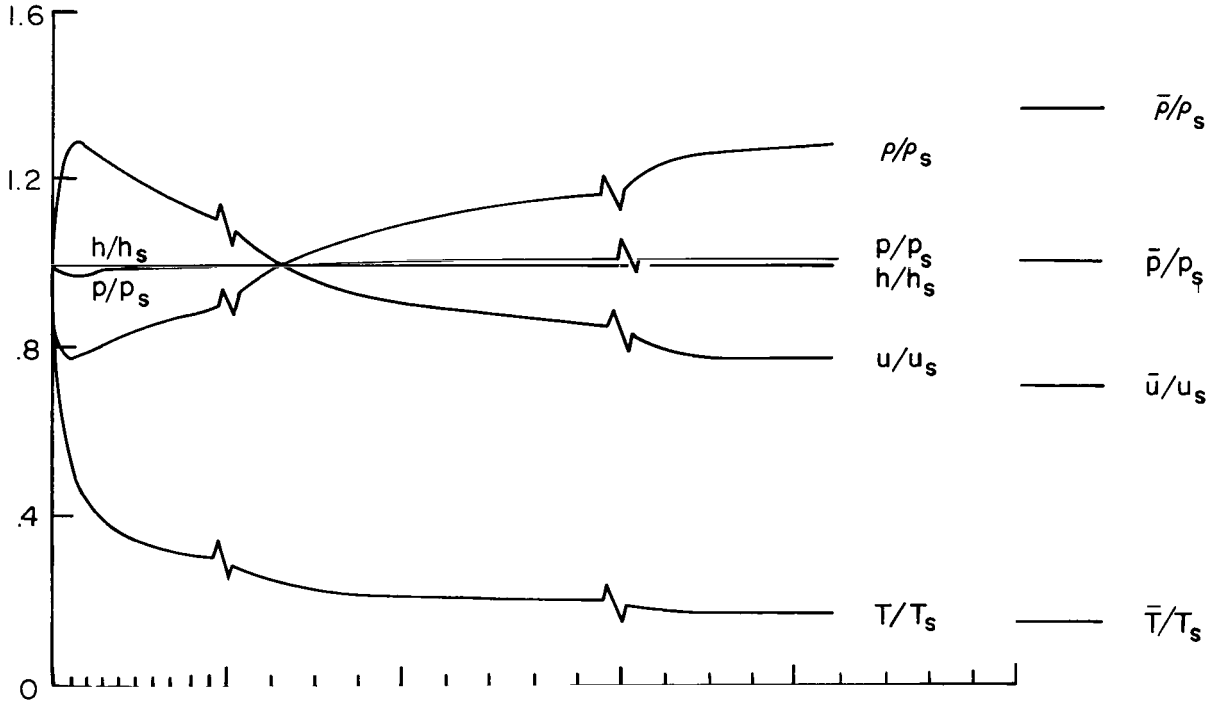

(a) Thermodynamic and flow properties.

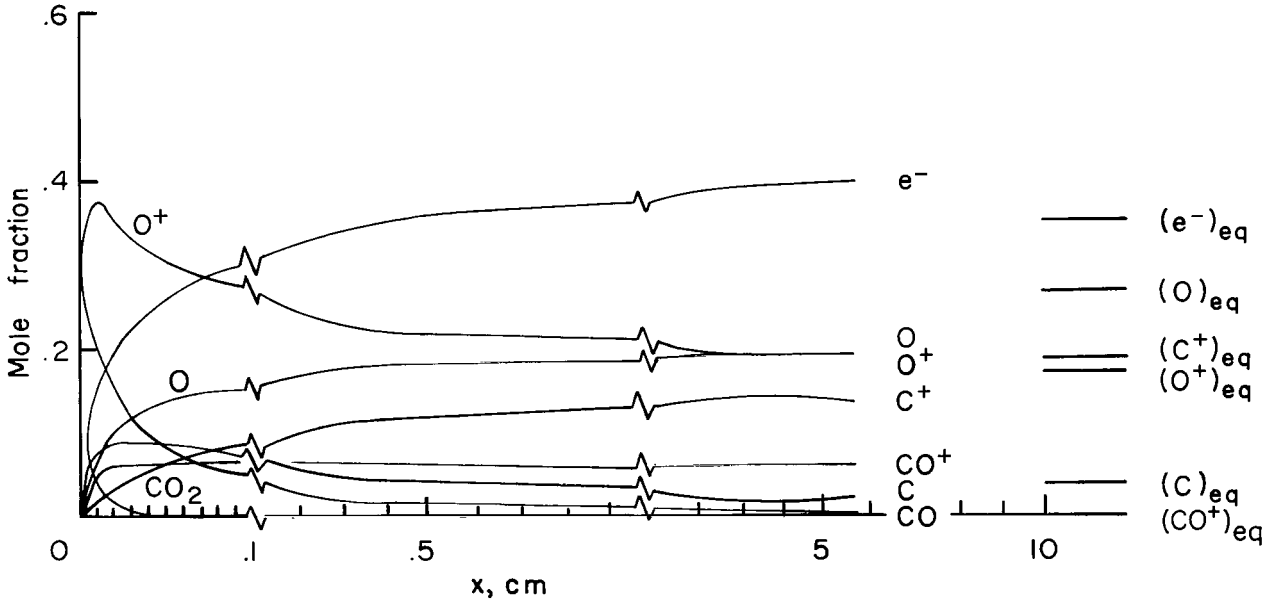

(b) Species concentration.

Figure 18.- Nonequilibrium profiles with electronic excitation; u_∞ = 15 km/sec, $\rho_\infty/\rho_O = 10^{-4}$.

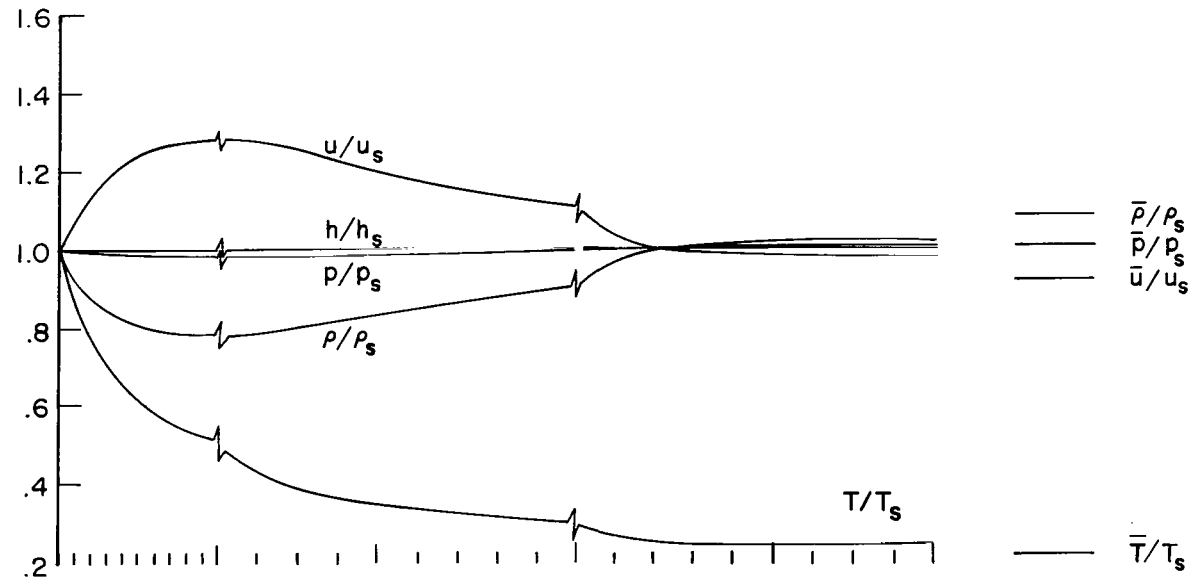

(a) Thermodynamic and flow properties.

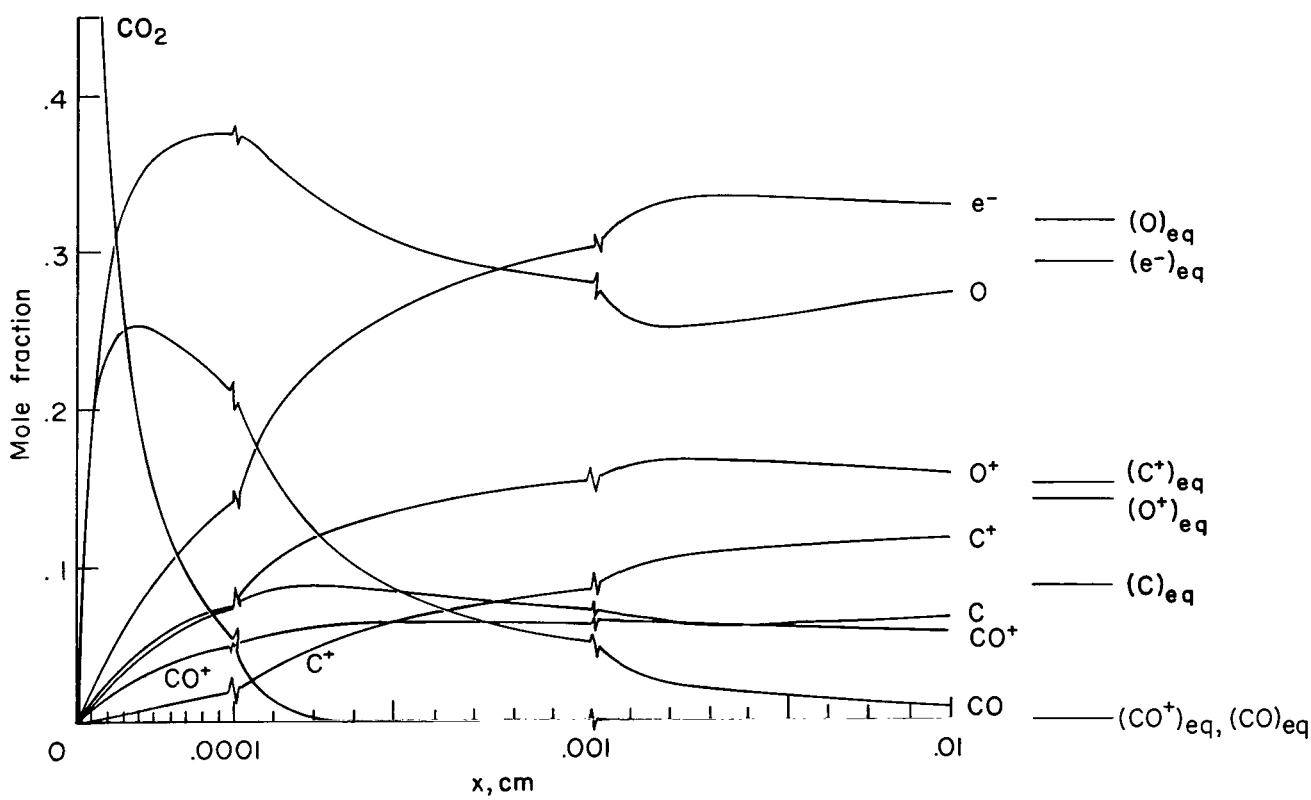

(b) Species concentration.

Figure 19.- Nonequilibrium profiles with electronic excitation; u_∞ = 15 km/sec, $\rho_\infty/\rho_O = 10^{-2}$.

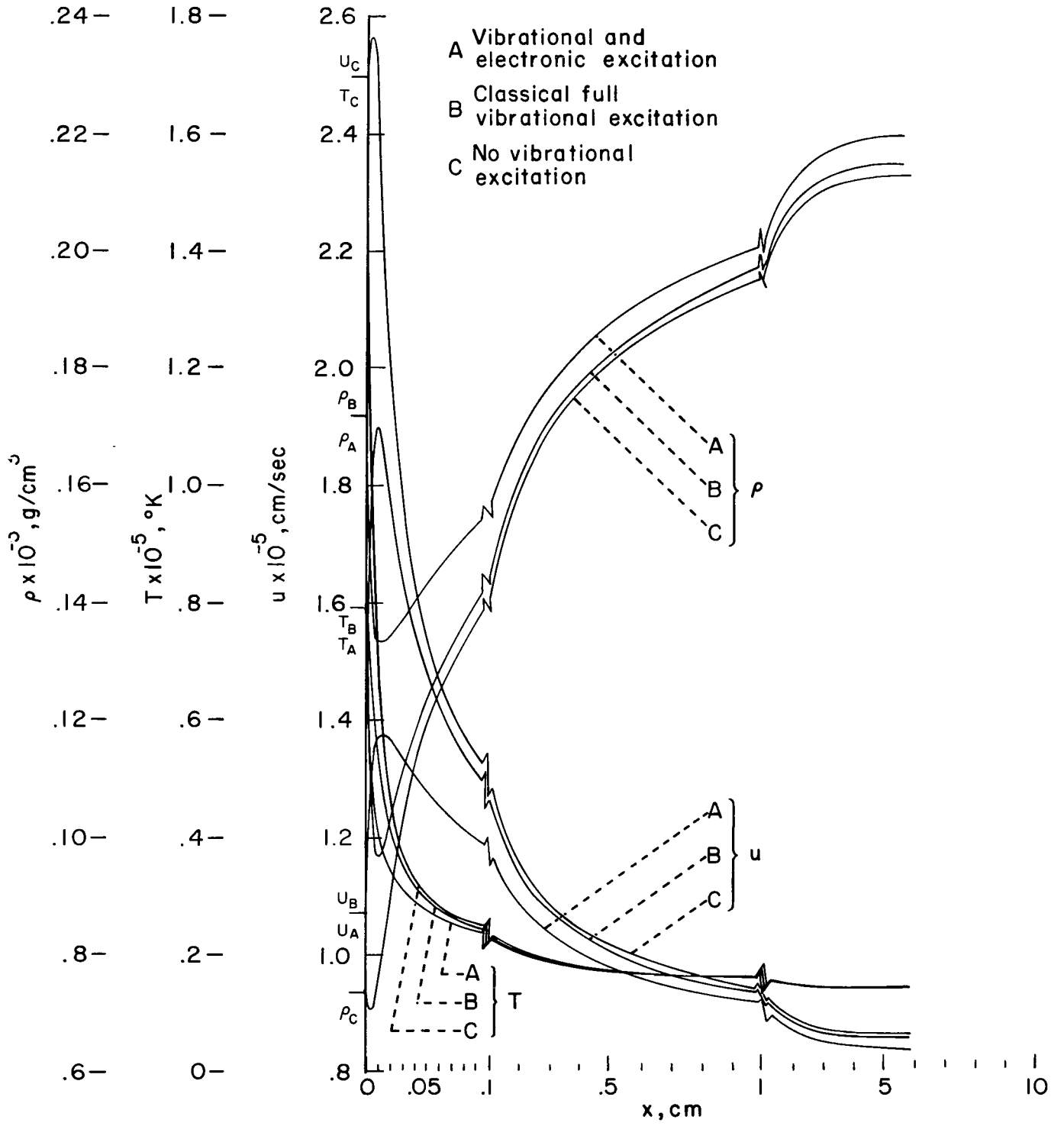

(a) Thermodynamic and flow-field profiles.

Figure 20.- Effect of state of internal excitation on chemical relaxation; u_∞ = 15 km/sec, $\rho_\infty/\rho_o = 10^{-4}$.

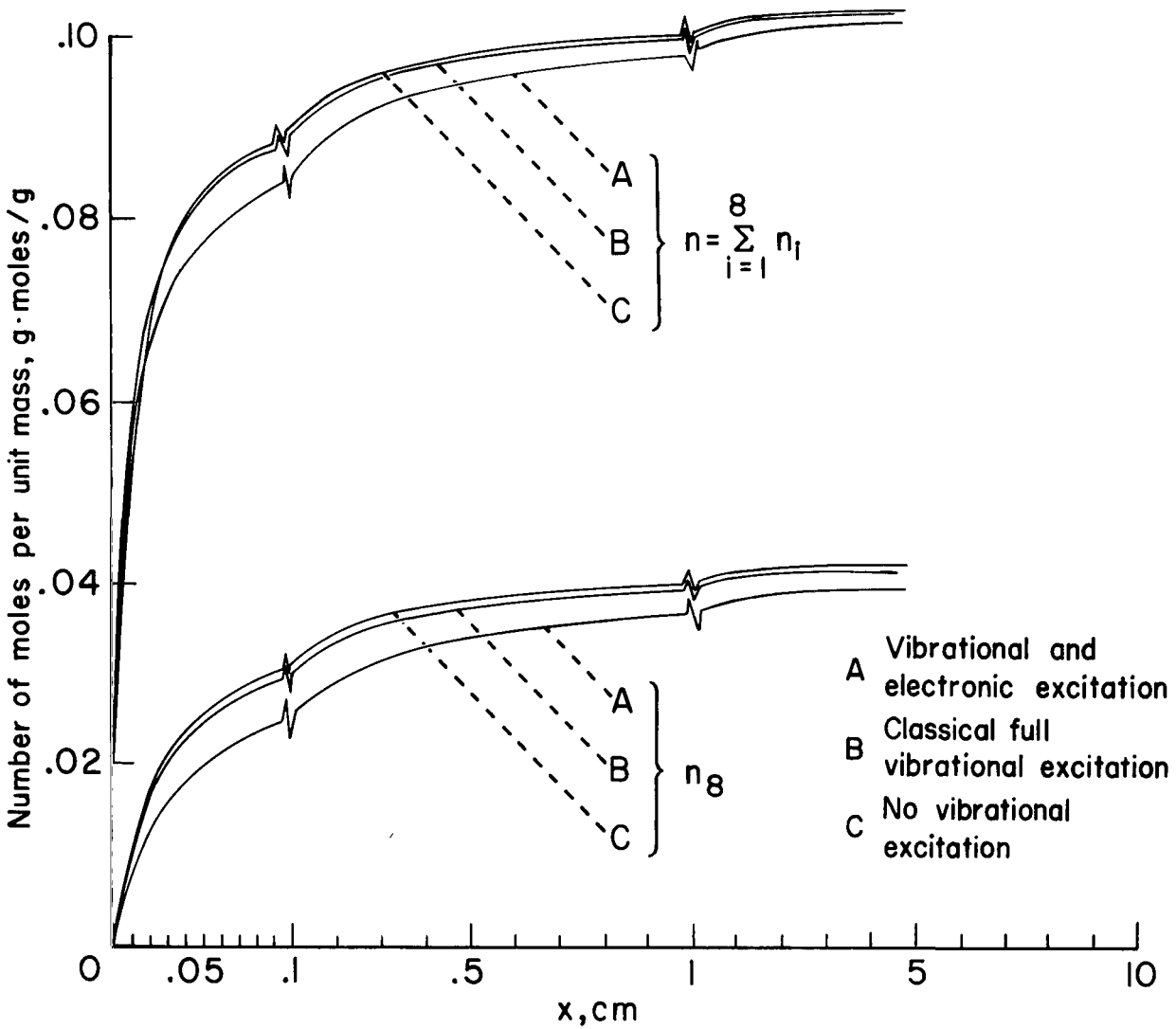

(b) Mole concentration profiles.

Figure 20.- Concluded.